Science Advances
AAAS

Manuscript Template

FRONT MATTER

Title

- m^{6}A RNA demethylase AtALKBH9B promotes mobilization of a heat-activated long terminal repeat retrotransposon in *Arabidopsis*
- RNA demethylation promotes retrotransposition

Authors

Wenwen Fan,[1,2]† Ling Wang,[1,2]† Zhen Lei,[1,2]† Hui Li,[1,2]† Jie Chu,[1,2]† Mengxiao Yan,[3] Yuqin Wang,[3] Hongxia Wang,[1,2,3] Jun Yang,[1,2,3] and Jungnam Cho[1,2,4,5]*

Affiliations

[1]National Key Laboratory of Plant Molecular Genetics, CAS Center for Excellence in Molecular Plant Sciences, Shanghai Institute of Plant Physiology and Ecology, Chinese Academy of Sciences, Shanghai 200032, China.
[2]University of Chinese Academy of Sciences, Beijing 100049, China.
[3]Shanghai Key Laboratory of Plant Functional Genomics and Resources, Shanghai Chenshan Botanical Garden, Shanghai 201602, China.
[4]CAS-JIC Centre for Excellence in Plant and Microbial Science, Shanghai 200032, China.
[5]Department of Biosciences, Durham University, Durham DH1 3LE, United Kingdom.
*Corresponding author (jungnam.cho@durham.ac.uk).
†These authors contributed equally to this work.

Abstract

Transposons are mobile and ubiquitous DNA molecules that can cause vast genomic alterations. In plants, it is well documented that transposon mobilization is strongly repressed by DNA methylation; however, its regulation at the posttranscriptional level remains relatively uninvestigated. Here, we suggest that transposon RNA is marked by m^{6}A RNA methylation and can be localized in stress granules (SGs). Intriguingly, SG-localized AtALKBH9B selectively demethylates a heat-activated retroelement, *Onsen*, and thereby releases it from spatial confinement, allowing for its mobilization. In addition, we show evidence that m^{6}A RNA methylation contributes to transpositional suppression by inhibiting virus-like particle assembly and extrachromosomal DNA production. In summary, this study unveils a previously unknown role for m^{6}A in the suppression of transposon mobility and provides insight into how transposons counteract the m^{6}A-mediated repression mechanism by hitchhiking the RNA demethylase of the host.

Teaser

Retrotransposon hijacks an RNA demethylase of the host to circumvent the RNA methylation-mediated repression.

MAIN TEXT

Introduction

Transposable elements (TEs or transposons) are DNA molecules that can move from one place to another and are widespread in most eukaryotic genomes (*1–3*). Two classes of

transposons have been identified: class I RNA transposons that move by a 'copy-and-paste' mechanism through an RNA intermediate and class II DNA transposons that move by a 'cut-and-paste' mechanism (*1*, *4*). Due to their potentially adverse effects on host genomes, most transposons are strongly repressed by epigenetic mechanisms, including DNA methylation and histone modifications (*5–9*). Despite their strong epigenetic repression, transposons can be activated by environmental challenges, which thereby bring about genetic diversity and adaptive changes of evolution (*1*, *10*, *11*). For example, a Ty1/Copia-like retrotransposon of *Arabidopsis* called *Onsen* can be transcriptionally activated by heat stress and confers heat responsiveness to genes located downstream of insertion positions (*12*, *13*).

It is well documented that *Onsen* is strongly suppressed by epigenetic pathways involving small interfering (si) RNAs (*12*, *14*, *15*). Recently, CHROMOMETHYLASE 3 (CMT3) was suggested to promote *Onsen* transcription by preventing CMT2-mediated CHH (H; A, T or C) methylation and histone H3 lysine 9 dimethylation (H3K9me2) accumulation at *Onsen* chromatin under heat stress (*16*). Similarly, histone H1 represses the expression of *Onsen* under heat stress and is required for DNA methylation (*17*). Whereas the repression of *Onsen* at the transcriptional level by DNA methylation is very well characterized, the regulation of *Onsen* RNA at the posttranscriptional level has not been extensively investigated.

Posttranscriptional RNA modification has emerged as a critical regulatory mark relevant to a variety of RNA processes (*18–21*). Its study is often referred to as epitranscriptomics, analogous to epigenetics. In fact, cellular RNAs contain at least 100 different kinds of posttranscriptional modifications, and N6-methyladenosine (m^6A) is the most abundant modification type present in mRNAs (*18*, *19*, *22*, *23*). In plants and other eukaryotes, m^6A methyltransferases catalyze RNA methylation at a highly conserved sequence motif, RRACH (R; G or A) (*24*, *25*). In *Arabidopsis*, it has been previously demonstrated that m^6A RNA methylation is critical for a variety of biological processes, including development, stress response and hormone signaling (*25–31*). Importantly, several studies also suggested that m^6A RNA modification regulates TEs; in mammalian cells, for instance, the m^6A writer complex and reader protein YTH domain containing 1 (YTHDC1) suppress the expression of endogenous retroviruses (*32*, *33*). In contrast, methyltransferase-like protein 3 (METTL3) promotes the transposition of long interspersed element-1 (L1), while RNA demethylase AlkB homologue 5 (ALKBH5) inhibits L1 mobility (*34*, *35*).

The *Arabidopsis* genome contains thirteen ALKBH homologous proteins (*36*), five of which exhibit a high level of similarity to ALKBH5 (*27*). To date, only two proteins, AtALKBH9B and AtALKBH10B, have been demonstrated to catalyze RNA demethylation (*27*, *37*). AtALKBH10B is involved in flowering time regulation and directly targets the transcripts of *FT*, *SPL3* and *SPL9* (*27*, *38*). *AtALKBH9B* is distinctively expressed in the cytoplasm, unlike other RNA demethylases (*36*, *37*). Previous studies suggested that AtALKBH9B regulates infection by alfalfa mosaic virus (*37*, *39*, *40*). Interestingly, AtALKBH9B colocalizes with stress granule (SG) and cytoplasmic siRNA body markers (*37*), potentially implying a functional association with RNA-mediated epigenetic silencing or RNA degradation pathways. Given the similarity of replication cycles between retroviruses and retrotransposons, TEs might also be subject to RNA methylation-mediated control; however, transposon regulation by m^6A RNA modification has not been explored in plants. In this work, we investigated the role of m^6A RNA

modification in the control of transposon suppression in *Arabidopsis*, which involves TE RNA localization in SGs. Intriguingly, a specific retroelement known as *Onsen* bypasses such m^{6}A-mediated suppression by exploiting the host-encoded RNA demethylase.

Results

Onsen RNA is m^{6}A-modified

It is well documented that plant transposons are massively derepressed by heat stress (*41*, *42*). Despite the strong transcriptional activation of TEs under heat, transposition events are rarely observed (*12*, *43*, *44*), implicating possible repressive mechanisms at the RNA level. Since previous studies in humans revealed the relevance of m^{6}A regulation in the control of retrotransposons, we hypothesized that plant transposons might be controlled by a similar mechanism. To test whether m^{6}A RNA modification plays a role in transposon regulation, we analyzed public datasets for m^{6}A-RNA immunoprecipitation sequencing (RIP-seq) data generated from *Arabidopsis* floral buds harvested before and after 3 hours (h) of heat treatment (*38*). Fig. 1A shows the distribution of m^{6}A enrichment across the transcribed regions, exhibiting a strong peak around the stop codon and a weaker peak at the transcriptional start site, which are consistent with the previously well-known pattern of m^{6}A (*24*, *25*, *27*, *28*, *45*). We identified almost 2,000 methylated RNAs that are specifically present in the heat stress conditions (Fig. 1B) and found that these transcripts were significantly overrepresented with transposons (Fig. 1C). In addition, our analyses of the public RNA-seq datasets generated from the same samples used in Fig. 1A also revealed that TE contains more transcripts with high m^{6}A peak numbers, including a retrotransposon family known as *Onsen* (Fig. 1D). These data collectively show that TE RNAs are more strongly modified by m^{6}A RNA methylation and partly suggest that m^{6}A RNA modification might be involved in the posttranscriptional suppression of transposon mobilization.

Onsen is a heat-activated retrotransposon and produces extrachromosomal linear (ecl) DNA, a pre-integrational reverse-transcribed product of a DNA intermediate that inserts into a new genomic position (*12*, *42*). *Onsen* exhibited a high level of m^{6}A along its RNA, with the most prominent peak close to the start codon (Fig. 1E). The *Arabidopsis* reference genome contains eight intact elements of *Onsen*, and all these elements displayed strong m^{6}A enrichment (Fig. 1F, fig. S1). To verify the m^{6}A RNA modification of *Onsen* RNA, an Oxford Nanopore Technologies direct RNA sequencing (ONT-DRS) experiment was also performed using the RNA extracted from the Col-0 seedlings heat-stressed for 24 h. ONT-DRS is able to detect modified bases in native RNA (*46*, *47*), and our result supports the presence of m^{6}A RNA modifications in *Onsen* RNA (Fig. 1E). We further confirmed the m^{6}A levels of *Onsen* in the 24 h-heat stressed Col-0 seedlings by qPCR, and a strong m^{6}A enrichment was detected in regions *B* and *C*, which is consistent with Fig. 1E (Fig. 1G). In summary, the heat-activated transposon *Onsen* is strongly marked by m^{6}A RNA methylation.

AtALKBH9B is an m^{6}A RNA demethylase that regulates *Onsen*

In search of possible regulators of *Onsen* RNA methylation, all known m^{6}A regulators were analyzed for their expression pattern under heat treatment using the public RNA-seq

datasets generated from the wild-type (wt) *Arabidopsis* plants treated with 3 or 24 h of heat stress (*38*, *44*). Most of the genes encoding m^6A writers, erasers, and readers were upregulated upon heat stress (fig. S2), possibly indicating a functional association of RNA methylation and the heat stress response. Among these genes, we focused on *AtALKBH9B*, which was previously suggested to regulate viral RNAs (*37*). Since TE RNAs share several cellular characteristics in common with viral RNAs, we hypothesized that *AtALKBH9B* might also regulate *Onsen* RNA. In line with this hypothesis, the expression patterns of *AtALKBH9B* and *Onsen* during a time course of heat treatment were similar, displaying a rather slow increase and peak at 24 h after heat stress (fig. S3).

To test whether *AtALKBH9B* is involved in *Onsen* RNA regulation, we first isolated a T-DNA insertional mutant, *atalkbh9b-1*, and generated a deletion mutant, *atalkbh9b-2*, using the CRISPR-Cas9 system (Fig. 2A, fig. S4A). The RNA levels of *Onsen* were strongly upregulated in both mutants under heat stress (Fig. 2B), and a similar pattern was also observed in RNA-seq data generated from the heat-stressed *atalkbh9b-1* mutant (Fig. 2C). We then expressed GFP-tagged AtALKBH9B in the *atalkbh9b-1* mutant and were able to detect the suppression of *Onsen* RNA to the wt level (Fig. 2D). In addition, previous studies suggested that *AtALKBH9B* and *AtALKBH10B* are expressed at high levels throughout various developmental stages, while other RNA demethylases are marginally expressed (*27*). The *atalkbh10b* mutants were thus tested for *Onsen* RNA levels; however, we were not able to detect any noticeable changes, suggesting that AtALKBH10B plays a negligible role in *Onsen* RNA regulation (fig. S5). We next performed m^6A-RIP-qPCR experiments using the heat-stressed wt and *atalkbh9b-1* mutant seedlings. Whereas no strong difference in the m^6A level was observed for a nonmethylated transposon in wt and *atalkbh9b-1* (fig. S6), the m^6A levels of *Onsen* RNA were significantly elevated in the *atalkbh9b-1* mutant (Fig. 2E), indicating that AtALKBH9B might cause the demethylation of *Onsen* RNA. To determine whether AtALKBH9B is a direct regulator of *Onsen* RNA, we carried out RIP-qPCR experiments using the *pAtALKBH9B::AtALKBH9B-GFP* transgenic line which expresses the tagged proteins at an equivalent level to the native AtALKBH9B (fig. S4B). Fig. 2F shows a substantial level of AtALKBH9B-GFP enrichment to *Onsen* RNA, while we were unable to observe any binding enrichment in the non-methylated RNAs (fig. S1, H and I). Together, these suggest that AtALKBH9B is an RNA demethylase that directly targets *Onsen* RNA.

Loss of *AtALKBH9B* results in reduced transposition of *Onsen*

Since the RNA levels of *Onsen* were increased in the *atalkbh9b* mutants, we speculated that the transpositional activity would also be increased in the *atalkbh9b* mutants. To directly determine the *Onsen* mobility, we first carried out amplification of linear extrachromosomal DNA (ALE)-qPCR experiments that can assess the pre-integrational DNA intermediate levels (*42*). Intriguingly, the eclDNA levels of *Onsen* were drastically reduced in the *atalkbh9b-1* mutant (Fig. 3A). Similar results were also observed in the experiments detecting the total DNA levels of *Onsen* in the heat-stressed *atalkbh9b-1* mutant (Fig. 3B). We then wanted to directly measure the insertional activity of *Onsen* in the *atalkbh9b-1* mutant, and for this, we performed droplet digital PCR (ddPCR) experiments to quantitatively determine the copy numbers of the *Onsen* retroelement (*48*). Since the mobilization of *Onsen* is hardly detectable in the wt background, plants were grown on the media containing α-amanitin and zebularine, which are known to enhance

Onsen retrotransposition activity (*43*). Surviving plants after heat stress were then grown to maturity, and seeds were collected from individual plants. Plants of the subsequent generation were subjected to ddPCR without heat stress treatment to assess the genomic copies of *Onsen*. As shown in Fig. 3C, the *atalkbh9b-1* mutant generated fewer new *Onsen* copies than the wt. We then tested the *alalkbh9b-1* mutant introduced in the *nrpd1a-3* mutant background in which *Onsen* can be mobilized. Consistently, the ddPCR data revealed that the loss of *AtALKBH9B* leads to compromised retrotranspositional activity (Fig. 3D). These data indicate that *AtALKBH9B* is required for *Onsen* mobilization.

AtALKBH9B and m^{6}A-methylated RNAs are localized to SGs under heat

Our results thus far indicated that the *atalkbh9b* mutant exhibits opposing patterns to different *Onsen* intermediates, i.e., increased RNA and reduced DNA levels. We speculated that such divergence might be caused by RNA sequestration that inhibits the conversion of RNA to DNA intermediates. Previous studies in humans demonstrated a strong association of methylated RNAs with SGs (*49*, *50*). An SG is an evolutionarily conserved intracellular compartment that is formed under stress conditions and stores proteins and RNAs (*51–54*). We therefore hypothesized that hypermethylated *Onsen* RNA in *atalkbh9b* might be localized in SGs and was precluded from where eclDNA production occurs. To test this hypothesis, we first investigated whether the AtALKBH9B protein was localized in SGs. We expressed AtALKBH9B-GFP in tobacco leaves along with SUPPRESSOR OF GENE SILENCING 3 (SGS3)-TdTomato as an SG marker. As shown in Fig. 4A, cytoplasmic foci of SGs were formed under heat stress, and AtALKBH9B-GFP colocalized with SGS3-TdTomato. The association of AtALKBH9B with SGs was further examined in double transgenic *Arabidopsis* plants expressing both AtALKBH9B-GFP and SGS3-TdTomato. Consistent with Fig. 4A, AtALKBH9B-GFP was in cytoplasmic foci along with SGS3-TdTomato in *Arabidopsis* root epidermal cells (Fig. 4, B and C). We further investigated the interactome of AtALKBH9B by performing IP/mass spectrometry (MS) experiments using *Arabidopsis* transgenic plants expressing AtALKBH9B-GFP. Our IP/MS data identified many proteins that were previously known as SG components (Fig. 4D, fig. S7, table S1, table S2). Notably, the YTH domain-containing m^{6}A reader proteins ECT1 and ECT2 were identified in the AtALKBH9B interactome (Fig. 4D, table S1, table S2). It is also worth noting that a substantial fraction of AtALKBH9B-interacting proteins is commonly found in the previously reported SG proteome data (table S2) (*55*). Among those proteins that are in both the AtALKBH9B interactome and stress granule proteome, ECT2 was chosen for further testing of its interaction with AtALKBH9B. We performed split luciferase assay experiments in tobacco leaves and observed a notable protein-protein interaction between AtALKBH9B and ECT2 (Fig. 4E). Two other SG marker proteins, UBP1b and PAB2, were also tested for their interaction with 9B in split luciferase assays, and we were able to detect the interaction between AtALKBH9B and SG marker proteins (fig. S8). Overall, AtALKBH9B is localized to SGs and interacts with multiple SG components.

We next investigated whether m^{6}A-methylated RNAs are preferably localized to stress granules in *Arabidopsis*. For this, we carried out RNA dot blot experiments with an m^{6}A antibody using the RNAs extracted from the SG fraction of the heat-stressed *atalkbh9b-1* mutants (fig. S9). Compared to total RNA, SG RNA showed a higher level of m^{6}A RNA

modification (Fig. 5, A and B), which is consistent with what is known in mammalian SGs (*49*, *50*). RNA-seq was also performed using the total and SG RNAs derived from the heat-stressed wt and *atalkbh9b-1* mutant. We observed that the SG-enriched RNAs contained a higher number of m^{6}A peaks than total RNAs (Fig. 5C). To directly detect the m^{6}A RNA modification in the SG-enriched transcripts, the ONT-DRS experiment was performed. Fig. 5D shows that the transcripts that were strongly associated with SG exhibited higher levels of m^{6}A RNA methylation in the SG fraction. We then identified the transcripts upregulated in *atalkbh9b-1* from the RNA-seq data shown in Fig. 5C and compared their SG enrichment. When compared with randomly selected RNAs, the AtALKBH9B-regulated transcripts showed stronger SG enrichment (Fig. 5E). A similar result of stronger SG enrichment was also observed for the transcripts that were hypermethylated in *atalkbh9b-1* (Fig. 5F). SG enrichment was also compared in the wt and *atalkbh9b* for the hypermethylated transcripts, and we observed a marked increase in SG enrichment in the *atalkbh9b-1* mutant (Fig. 5G). The enhancement of SG localization of *Onsen* RNA in *atalkbh9b-1* was further validated by qPCR using *CCR2* as a negative control (fig. S10). Fig. 5H shows that the SG enrichment of *Onsen* RNA was increased in the *atalkbh9b-1* mutant. We also tested the mutants for SG components and observed that the *Onsen* RNA levels were decreased in these mutants (fig. S11), which partly indicates that SG stabilizes *Onsen* RNA. In short, the AtALKBH9B protein and m^{6}A-methylated transcripts are localized in cytoplasmic SGs under heat stress.

m^{6}A inhibits VLP assembly and eclDNA production

We have demonstrated that m^{6}A-methylated *Onsen* RNA is localized in SGs and that AtALKBH9B demethylates it, allowing for its mobilization. It is, however, important to note that neo-insertions of *Onsen* are hardly detectable in the wt background (*12*, *43*). We thus postulated additional inhibitory effects of m^{6}A RNA modification on the retrotransposition of *Onsen* other than RNA sequestration to SGs. Since the production of pre-integrational DNA intermediates occurs in virus-like particles (VLPs) and the physical interaction between template RNA and retroelement-encoded Gag protein is the first step of it (*4*, *42*), we tested whether the methylation status of RNA influences the affinity of Gag with RNA. A fluorescence polarization assay was carried out to determine the in vitro binding activity of Gag using RNA oligonucleotides that are identical in sequence but differ in m^{6}A methylation status. As shown in Fig. 6A, the m^{6}A-modified RNA exhibited an increased *Kd* value compared to the nonmethylated RNA, suggesting that m^{6}A inhibits the binding to Gag. We further examined the interaction of Gag and *Onsen* RNA by performing RIP-qPCR experiments using Gag-GFP-expressing transgenic *Arabidopsis* plants (fig. S12). Gag-GFP showed strong binding enrichment to *Onsen* RNA; however, when Gag-GFP was expressed in the *atalkbh9b-1* mutant background, the binding enrichment was drastically reduced (Fig. 6B). In addition, we speculated that m^{6}A RNA methylation might interfere with the reverse transcription process. To test this possibility, partial *Onsen* RNA was in vitro transcribed in the presence or absence of m^{6}A substrate and subjected to the reverse transcription reaction. Consistent with previous studies suggesting that reverse transcriptional activity can be compromised by RNA modifications (*56*, *57*), the m^{6}A-modified RNA showed higher Cq values (fig. S13), which indicates that RNA methylation inhibited cDNA production. Together, these data suggest that m^{6}A RNA methylation contributes to retrotransposition suppression by inhibiting VLP assembly and eclDNA production.

Discussion

In this study, we showed that the heat-activated retrotransposon *Onsen* is m^{6}A-modified and localized to cytoplasmic SGs (Fig. 1, Fig. 5). m^{6}A RNA methylation not only leads to spatial constraints preventing RNA maturation to eclDNA but also biochemically inhibits VLP assembly and reverse transcription (Fig. 6, fig. S13). Importantly, the SG-localized RNA demethylase AtALKBH9B directly targets *Onsen* RNA and allows it to complete the retrotranspositional process (Fig. 2, Fig. 3). Our study provides insight into the biological role of SGs as sites for the seclusion of transposon RNAs and thus the suppression of their mobility. This notion is partially in agreement with previous work in mammals that suggested the m^{6}A-mediated inhibition of transposons through RNA destabilization, which presumably occurs in cytoplasmic RNA granules (*32*, *33*). However, the discrepancy between the roles of m^{6}A in *Arabidopsis* and those in animals is that it does not trigger strong RNA decay but is associated with RNA stabilization (*24*, *58*). Our data also showed that the depletion of SG components results in the reduction of *Onsen* RNA levels (fig. S11), indicating that SG enhances RNA stability. Together, these results indicate that m^{6}A RNA methylation of *Onsen* guides RNA to SGs without compromising their RNA stability.

m^{6}A RNA methylation presumably occurs co-transcriptionally in the nucleus by RNA methyltransferases that broadly target nascent transcripts with limited specificity (*59–61*), and indeed, more than ten thousand transcripts were found to be methylated in our study (Fig. 1, fig. S14). Intriguingly, SG localization seems to occur selectively in a subset of m^{6}A-modified transcripts (Fig. 5, fig. S14), although the responsible m^{6}A reader protein is unknown. A recent study on ECT2, a m^{6}A-binding and SG-localized protein, hints at possible mechanisms for the selective guidance of m^{6}A-modified transcripts to SGs (*62*). The ECT2-binding transcriptome revealed a strong sequence bias towards U that is enriched around m^{6}A-modified sites (*62*). Interestingly, a similar sequence bias of high AU contents in transposon RNA was shown in our previous report (*54*). Therefore, it can be speculated that certain sequence features recognized by m^{6}A reader proteins provide selectivity to m^{6}A-mediated SG localization.

Furthermore, we noticed that AtALKBH9B regulates only a few transcripts in SGs including *Onsen* (fig. S14). AtALKBH9B was previously characterized to localize to SGs and facilitate viral infectivity (*37*), which is similar to what we observed for the *Onsen* retroelement. In fact, AtALKBH9B is peculiar and distinct from AtALKBH10B, the other active RNA demethylase in *Arabidopsis*. For example, unlike many other RNA demethylases, AtALKBH9B is localized to cytoplasmic foci and regulates relatively fewer transcripts (*27*, *36*). Additionally, we showed that the *Onsen* transcript levels were not altered in the *atalkbh10b* mutants and were controlled specifically by AtALKBH9B (Fig. 2, fig. S5). These results imply the functional diversification of RNA demethylases and indicate that AtALKBH9B might have evolved to preferentially target nonnative and invasive genetic elements such as retroviruses and retrotransposons. Further investigation of the biochemical characterization of the AtALKBH9B protein will be required to understand target-specific RNA demethylation. In addition, since several m^{6}A reader proteins were identified as AtALKBH9B-interacting partners (Fig. 4), it will also be important to test whether these proteins have a role in the specific RNA target recognition of AtALKBH9B.

In summary, mobile genetic elements are subject to multilayered repression at the transcriptional and posttranscriptional steps. Our work suggests a previously unknown mechanism for the suppression of transposon mobilization that involves m^6A RNA methylation and the localization of TE RNA in SGs. Importantly, the retrotransposon *Onsen* provides an intriguing example of adopting a host factor to bypass such suppression.

Materials and Methods

Plant materials and growth condition

Arabidopsis mutants used in this study are in the Col-0 background and were obtained from the Nottingham Arabidopsis Stock Centre (*atalkbh9b-1*, SALK_015591C; *g3bpl-1*, SALK_011708; *sgs3-14*, SALK_001394; *rdr6-11*, CS24285; *ago7-1*, SALK_037458; *nrpd1a-3*, SALK_128428). To induce de novo mutations in *AtALKBH9B*, a CRISPR-Cas9 vector was constructed by cloning three sgRNAs (sequences are provided in Table S3) into the Cas9-containing binary vector. The oligonucleotides encoding the sgRNAs were first cloned into the pENTR_L4_R1, pENTR_L1_L2 and pENTR_R2_L3 entry vectors at the BbsI sites. The entry vectors containing the sgRNAs were then cloned into the destination vector by the LR recombination reaction using the MultiSite Gateway Pro kit (Thermo Fisher Scientific). The resulting vector was transferred to *Agrobacterium tumefaciens* strain GV3101 and transformed into Col-0 *Arabidopsis* plants. As the vector carries a GFP fluorescence gene driven by a seed coat-specific promoter, the collected T1 seeds were illuminated with the LUYOR-3415RG Dual Fluorescent Protein Flashlight to identify the transformants. T-DNA was segregated out at T2 generation by genotyping the Cas9-encoding gene and the gene editing events were identified by PCR amplifying the targeted region followed by Sanger sequencing (Table S3). For a mutant complementation test of *atalkbh9b-1*, the fluorescence-tagged AtALKBH9B transgenic plants were obtained by constructing a vector *pAtALKBH9B::AtALKBH9B-GFP:tHSP18.2*. Each fragment was PCR amplified using the primers listed in Table S3 and was cloned into the pCAMBIA1300 using the T4 DNA ligase (NEB). The construct was transformed into the *atalkbh9b-1* mutant, and the transgenic lines were identified for homozygosity at T3 generation.

Arabidopsis seeds were surface sterilized in 75% ethanol for 15 min, washed with 100% ethanol for 1 min, and planted on half-strength MS media (including 1% sucrose). Prior to germination, seeds were stratified for 2 days at 4 °C under the dark condition and moved to a growth chamber set at 22 °C and 12-h light/12-h dark cycle. For the heat stress treatment, plants were grown for 6 days at 22 °C and then treated with heat stress of 37 °C for 24 h.

RT-qPCR

Plant samples were flash frozen and ground in liquid nitrogen. Total RNA was isolated using the TRIzol Universal Reagent (Tiangen). Briefly, 100 mg of the ground tissue powders were resuspended in 1 mL of TRIzol reagent, incubated at room temperature for

5 min, and then centrifuged at top speed for 10 min at 4 °C. The supernatant was mixed vigorously with chloroform and centrifuged at top speed for 10 min at 4 °C. The upper phase was mixed with the same volume of isopropanol and incubated at -80 °C for 10 min. The RNA was precipitated by centrifugation and the pellet was washed with 1 mL of 75% ethanol.

The first-strand cDNA synthesis was performed using 500 ng of RNA by the ReverTra Ace qPCR RT Master Mix with gDNA Remover (Toyobo). The resulting cDNA was diluted four-fold with DEPC-treated water and 1.5 μL was used for a 20-μL qPCR reaction mixture. The qPCR was carried out using ChamQ Universal SYBR qPCR Master Mix (Vazyme) in the CFX96 Connect Real-time PCR Detection system (BioRad). *Actin2* was used as the internal control and the sequences of the primers used for RT-qPCR are provided in Table S3.

RIP-qPCR

Direct binding of a protein to RNA was assessed by RIP-qPCR experiments. 7-d-old seedlings heat-stressed at 37 ℃ for 1 day were flash frozen and ground in liquid nitrogen. Over 2 g of frozen powder was homogenized in 6 mL of extraction buffer [100 mM Tris-HCl (pH 7.5), 150 mM NaCl, 0.5% IGEPAL (Sigma), and 1% plant protease inhibitor cocktail (MedChem Express)]. The crude extract was incubated at 4 ℃ for 30 min with shaking and then centrifuged for 30 min at 18,000 *g* at 4 °C. 87.5 μL of 40 U/μL RNase inhibitor (ABclonal) and 25 μL of GFP-trap magnetic beads (Chromotek) was added to 3.5 mL of the supernatant and incubated overnight at 4 °C. 350 μL of the supernatant was kept as an input sample and stored at -80 ℃ freezer until use. After washing four times with 1 mL extraction buffer, the beads were resuspended in 150 μL of the proteinase K buffer (15 μL 10% SDS, 18 μL 10 mg/mL proteinase K and 117 μL extraction buffer) and incubated for 30 min at 55 °C. RNA was then extracted by adding 400 μL phenol:chloroform:isopropanol. The mixture was vortexed rigorously for 15 sec and centrifuged at 14,000 *g* for 10 min at room temperature. 350 μL of the aqueous phase was mixed with 400 μL of chloroform, vortexed, and centrifuged at 14,000 *g* for 10 min at room temperature. 300 μL of the aqueous phase was carefully moved to a new tube and added with 30 μL of 3 M sodium acetate (pH 5.2) and 750 μL of 100% ethanol. The mixture was incubated at -80 °C overnight and centrifuged at 14,000 *g* for 30 min at 4 °C. The pellet was washed with 80% ethanol, air-dried, and resuspended in 15 μL of RNase-free water. The input fraction was subjected to the same procedure to extract RNA. The extracted RNAs were reverse-transcribed and analyzed in qPCR as described above in RT-qPCR (the oligonucleotide sequences are provided in Table S3). The *OnsenLTR::Gag-GFP* was constructed by modifying the pGPTVII binary vector (*44*) using the primers listed in Table S3. The construct was transformed into Col-0 *Arabidopsis* plants and introduced to the *atalkbh9b-1* mutant by genetic cross.

The m^6A enrichment experiment was performed as described previously with minor modifications (*63*) and the Magna RIP™ RNA-Binding Protein Immunoprecipitation Kit (Merck) was used following the manufacturer's instruction. Briefly, 300 μg of total RNA was randomly fragmented into 250-nucleotide fragments by RNA fragmentation reagents (for 1 mL 10X reagents: 800 μL 1 M Tris-HCl (pH 7.0), 100 μL 1 M ZnCl2, 100 μL RNase-free H2O). Fragmented RNA was precipitated using 2.5 volume of ethanol, 1/10

volume of 3 M NaOH, 100 μg/mL glycogen at -80 °C overnight. After centrifugation at 14,000 *g* for 10 min, the pellet was resuspended in 55 μL RNase-free H2O. 5 μL of RNA was kept as the input sample and the remaining RNA was incubated with 5 μg m^6A-specific antibody (cat. 202003, Synaptic Systems) overnight at 4 °C. The m^6A-containing fragments were pulled down with magnetic beads. The beads were then washed five times using 500 μL of cold RIP Wash Buffer, re-suspend in 150 μL of proteinase K buffer (117 μL of RIP Wash Buffer, 15 μL of 10% SDS, 18 μL of 10 mg/mL proteinase K), and incubated at 55 °C for 30 min with shaking. After incubation, the beads were separated on magnetic rack and the supernatant was mixed with 250 μL of RIP Wash Buffer. 400 μL of phenol:chloroform:isoamyl alcohol was added and the mixture was centrifuged at 14,000 g for 10 min at room temperature. 350 μL of the aqueous phase was then mixed with 400 μL of chloroform, and the mixture was centrifuged at 14,000 *g* for 10 min at room temperature. 300 μL of the aqueous phase was mixed with 50 μL of Salt Solution I, 15 μL of Salt Solution II, 5 μL of Precipitate Enhancer and then 850 μL of absolute ethanol. The mixture was stored at -80 °C overnight to precipitate the RNA. Then, the mixture was centrifuged at 14,000 *g* for 30 min at 4 °C and the pellet was washed with 80% ethanol. After centrifugation at 14,000 *g* for 15 min at 4 °C, the pellet was resuspended in 20 μL of RNase-free H2O. The extracted RNAs were reverse-transcribed and analyzed in qPCR as described above in RT-qPCR (the oligonucleotide sequences are provided in Table S3).

ALE-qPCR

ALE-qPCR was performed as previously described (*42*, *64*). Genomic DNA was extracted using a DNeasy Plant Mini Kit (Qiagen) following the manufacturer's instruction. 200 ng of genomic DNA and 1 pg of PCR-amplified *Evade* DNA was used for ligation with 0.5 μL of 40 μM adapter DNA overnight at 16 ℃ (the sequences are provided in Table S3). The adapter-ligated DNA was purified by AMPure XP beads (Beckman Coulter) at a 1:0.5 ratio. In vitro transcription reactions were performed using a Standard RNA Synthesis Kit (NEB). 1 μg of purified RNA was subjected to reverse transcription using a Transcriptor First Strand cDNA Synthesis Kit (Roche) and 1 μL of RNase A/T1 (Thermo Fisher Scientific) was added to digest non-templated RNA for 30 min at 37 °C. Subsequently, qPCR was performed as described above (the oligonucleotide sequences are provided in Table S3).

Induction of *Onsen* retrotransposition

To detect the retrotransposition of *Onsen*, *Arabidopsis* seedlings were grown in the media containing zebularine (Sigma) and α-amanitin (MCE), and then heat-stressed as described above. The chemical reagents were prepared by filter-sterilization (zebularine, 5 mg/mL in DMSO; α-amanitin 1 mg/mL in water) and used at the concentrations indicated in the previous study (*43*). The heat-stressed plants were transferred to soil and grown to maturity under the 16-h light /8-h night cycle at 22 °C, and the seeds were harvested from individual plants. DNA was extracted from a whole seedling that was randomly selected and subjected to either droplet digital PCR or whole-genome resequencing. *nrpd1a-3 atalkbh9b-1* double mutant was identified in F2 segregation population derived from a

cross of two single mutants. Plants containing the *nrpd1a-3* mutation were grown in the media without zebularine and α-amanitin.

Droplet digital PCR

The ddPCR experiments were carried out as previously described with minor modifications (*48*). Genomic DNA was extracted using a N96 DNAsecure Plant Kit (Tiangen) following the manufacturer's instruction. 100 ng of genomic DNA was digested using AluI for 4 h at 37 ℃. The digested DNA was diluted to 0.15 ng/μL using the Qubit4 DNA quantification system (Thermo Fisher Scientific) and the Probe ddPCR SuperMix mixture was prepared (Targeting One; 15 μL 2x SuperMix, 2.4 μL (10 μM) for each primer, 0.75 μL FAM-Probe (10 μM), 0.75 μL HEX-Probe (10 μM), 3.9 μL diluted DNA totaling 30 μL). Droplets were generated using the Drop maker (Targeting One) and PCR was performed as following: 95 °C for 10 min; then 55 cycles of 94 °C for 30 sec and 56.8 ℃ for 30 sec; 98℃ for 10 min. PCR products were read by Chip reader system (Targeting One). *CBF2* was used as the internal single-copy control. The oligonucleotide sequences are provided in Table S3.

Stress granule enrichment

Enrichment of cytoplasmic RNA granules was performed following the previously described method (*54*, *65*). Briefly, 2 g of seedlings was ground in liquid nitrogen and resuspended in 5 mL of lysis buffer [50 mM Tris–HCl (pH 7.4), 100 mM KOAc, 2 mM MgOAc, 0.5 mM dithiothreitol, 0.5% NP40, complete EDTA-free protease inhibitor cocktail (Roche), and 40 U/mL RNasin Plus RNase inhibitor (Promega)]. The mixture was filtered through four layers of Miracloth (Sigma-Aldrich) and centrifuged at 4,000 *g* for 10 min at 4 °C. The supernatant was removed, and the pellet was resuspended in 2 mL of lysis buffer. The samples were again centrifuged at 18,000 *g* for 10 min at 4 °C. The pellet was resuspended in 2 mL of lysis buffer, vortexed and centrifuged at 18,000 *g* at 4 °C for 10 min. The supernatant was discarded, and the pellet was resuspended in 1 mL of lysis buffer. After a brief centrifugation at 850 *g* for 10 min at 4 °C, the RNA granule fraction in the supernatant was collected for RNA extraction. To verify the SG enrichment, we generated the transgenic *pUBQ10::mCherry-UBP1B Arabidopsis* plants. Briefly, the genomic DNA of *UBP1B* was cloned into pCAMBIA1300 that contains N-terminal mCherry tag and introduced to Col-0 (sequences of primers used for cloning are provided in Table S3). Validation of the enrichment of stress granules was performed by western blots using the anti-Actin (26F7, Abmart, 1:1000) and anti-SGS3 (ref.(*66*), 1:1000) antibodies.

RNA dot blot

The extracted total and SG RNA was serially diluted and spotted on PVDF membrane (Bio-Rad). The membrane was soaked in 1-(3-Dimethylaminopropyl)-3-ethylcarbodiimide hydrochloride (EDC, Thermo Fisher Scientific) solution [125 mM 1-methyl Imidazole

(pH 8), 31.375 mg/mL EDC] and incubated at 65 ℃ for 2 h for cross-linking. The cross-linked membrane was washed four times with TBST buffer [150 mM NaCl, 20 mM Tris-HCl (pH 8.0), 0.05% Tween]. After blocking with 5% skim milk, the membrane was incubated in TBST buffer containing anti-m^{6}A antibody (Synaptic Systems) overnight at 4 ℃ with gentle agitation. Subsequently, the membrane was washed with TBST buffer four times and incubated in TBST buffer containing HRP-conjugated anti-rabbit IgG (Abmart) at room temperature for 1 h. Pour out the secondary antibody, add TBST, wash 4 times, 5 min each time. Chemiluminescence of the blot was detected using Omni-ECLTM Femto Light Chemiluminescence kit (EpiZyme) and images were acquired by Tanon-5200 (Tanon).

Next-generation sequencing

mRNA was purified from 3 μg of total RNA using the poly(T) oligo-attached magnetic beads (Thermo Fisher Scientific). Library preparation was performed using the NEBNext Ultra RNA Library Prep Kit (NEB) following the manufacturer's instructions. Sequencing was performed on an Illumina NovaSeq 6000 platform, and 150-bp paired-end (PE150) reads were generated.

For the data analysis, the raw sequences were processed using Trimmomatic (version 0.39) (*67*) to remove the adapter and low-quality sequences. Trimmed reads were then aligned to the *Arabidopsis* reference genome (TAIR10) with default settings using Hisat2 (version 2.2.1) (*68*). The FPKM values of genes and TEs were calculated by StringTie (version 2.1.7) (*69*). TEs that are annotated as genes in TAIR10 annotation were used in our analysis. Visualization of the sequencing data was performed using the Integrative Genomics Viewer (IGV) (*70*). For the m^{6}A peak calling, MACS2 (version 2.2.7.1) (*71*) was run with the following parameters; --nomodel,--extsize 50, -p 5e-2, and -g 65084214 (the -g option accounts for the size of the *Arabidopsis* transcriptome). The m^{6}A peaks detected in both biological replications were chosen and used in the subsequent analyses. NGS data generated in this study is summarized in Table S4.

Oxford Nanopore direct RNA sequencing

Total RNA was isolated by Trizol (Qiagen) and poly(A) RNA was purified using Dynabeads mRNA Purification Kit (Invitrogen) following the manufacturer's instructions. The quality and quantity of poly(A) mRNA was assessed using both the NanoDrop 2000 spectrophotometer and Qubit. The library was prepared using a direct RNA sequencing kit (Nanopore, SQK-RNA002), loaded onto an R9.4 Flow Cell (Flow cell type FLO-MIN106) and sequenced on a GridION device for 48 h.

The raw nanopore signals were converted to base sequences by Guppy (v4.2.3) using high-accuracy base calling model. The reads with a mean quality score greater than 7 were aligned to the *Arabidopsis* transcriptome (TAIR10 cDNA FASTA) using Minimap2 (v2.24-r1122) (*72*) with the following parameters: -ax map-ont -p 0 -N 10. NanoCount (v1.0.0.post6) (*73*) was used to get TPM value and --max_dist_3_prime was set to -1. DENA was adopted to identify m^{6}A sites. Sites supported by at least 10 reads and

modification rate more than 0.1 were kept as m^6A sites. The coordinates of m^6A sites on transcriptome were converted to genome coordinate by "mapFromTranscripts" from GenomicFeatures package. The distribution of m^6A on transcripts was checked by Guitar package (*74*). For each transcript, m^6A level was defined as an average m^6A ratio from all modified sites.

Confocal microscopy

To determine the subcellular localization of SGS3 and AtALKBH9B proteins, the pGPTVII binary vector was modified to generate *pUBQ10::SGS3-TdTomato* and *pUBQ10::AtALKBH9B-GFP* constructs. The CDS of AtALKBH9B and SGS3 were amplified from Col-0 cDNA using KOD-Plus-Neo (Toyobo) (primers are listed in Table S3). The vectors were transformed into Col-0 *Arabidopsis* plants, which were selected on 1/2 MS plates containing 10 μg/mL Glufosinate ammonium (Coolaber) and further confirmed by PCR using the primers targeting GFP and TdTomato (listed in Table S3). The *AtALKBH9B-GFP SGS3-TdTomato* double transgenic plant was generated from genetic crossing and identified by PCR-based genotyping in F2 populations. The transgenic plants were heat-stressed at 37 °C for 12 h and the fluorescence signals were detected by Zeiss LSM880 confocal microscopy. For the tobacco transient expression experiments, the constructs were expressed along with P19 in tobacco leaves. Tobacco plants were heat-stressed at 37 °C for 12 h at 48 h after agro-infiltration.

IP-MS

The 7-d-old seedlings of *pUBQ10::AtALKBH9B-GFP* and *p35S::GFP* were treated with 1-d heat stress under 37 ℃, and immediately flash frozen. 1 g of ground powder was homogenized in 3 mL of IP buffer [20 mM HEPES (pH 7.4), 2 mM EDTA, 25 mM NaF, 1 mM Na3VO4, 10% Glycerol, 100 mM NaCl, 0.5% Triton X-100 and 1% plant protease inhibitor cocktail (MedChem Express)] and the mixture was rotated at 4 ℃ for 1 h. The crude extract was centrifuged for 20 min at 18,000 *g* at 4 °C. The immunoprecipitation was performed using 3 mL of plant extract mixed with 25 μL of GFP-trap magnetic beads (Chromotek) at 4 °C overnight. The beads were washed four times with 1 mL IP buffer and centrifuged for 1 min at 200 *g* at 4 ℃.

For protein digestion, 100 μg of protein was reduced with 2 μL 0.5 M Tris(2-carboxyethyl)phosphine (TCEP) at 37 °C for 60 min and alkylated with 4 μL 1 M iodoacetamide (IAM) at room temperature for 40 min in darkness. Five-fold volumes of cold acetone were added to precipitate protein at -20 °C overnight. After centrifugation at 12,000 *g* at 4 °C for 20 min, the pellet was washed twice using 1 mL pre-chilled 90% acetone aqueous solution. Then, the pellet was re-suspended with 100 μL 10 mM Triethylammonium bicarbonate (TEAB) buffer. Trypsin (Promega) was added at 1:50 trypsin-to-protein mass ratio and incubated at 37 °C overnight. The peptide mixture was desalted by C18 ZipTip and lyophilized by SpeedVac.

For nano-HPLC-MS/MS analysis, the peptides were analyzed by online nano flow liquid chromatography tandem mass spectrometry performed on an EASY-nanoLC 1200 system

(Thermo Fisher Scientific) connected to a Q Exactive™ Plus mass spectrometer (Thermo Fisher Scientific). Acclaim PepMap C18 (75 μm x 25 cm) was equilibrated with solvent A (A: 0.1% formic acid in water) and solvent B (B: 0.1% formic acid in ACN). 3 μL peptide was loaded and separated with 60 min-gradient at flow rate of 300 nL/min. The column temperature was 40 °C. The electrospray voltage of 2 kV versus the inlet of the mass spectrometer was used. The peptides were eluted using the following gradient: 0-3 min, 2-6% B; 3-42 min, 6−20% B; 42-47 min, 20-35% B; 47-48 min, 35-100% B; 48-60 min, maintained 100% B.

The mass spectrometer was run under data dependent acquisition (DDA) mode, and automatically switched between MS and MS/MS mode. The survey of full scan MS spectra (m/z 200-1800) was acquired in the Orbitrap with resolution of 70,000. The automatic gain control (AGC) target at 3e6 and the maximum injection time was 50 ms. Then, the top 20 most intense precursor ions were selected into collision cell for fragmentation by higher-energy collision dissociation (HCD) with the collection energy of 28. The MS/MS resolution was set at 17500, the automatic gain control (AGC) target at 1e5, the maximum injection time was 45 ms, isolation window was 2 m/z, and dynamic exclusion was 30 sec.

Tandem mass spectra were processed by PEAKS Studio (v.10.6, Bioinformatics Solutions Inc.). PEAKS DB was set up to search the uniprot_Arabidopsis_thaliana (v.201907, entries 27477) database assuming trypsin as the digestion enzyme. PEAKS DB was searched with a fragment ion mass tolerance of 0.02 Da and a parent ion tolerance of 7 ppm. Carbamidomethylation (C) was specified as the fixed modification. Oxidation (M), Deamidation (NQ), and Acetylation (K) were specified as variable modifications. The peptides with -10logP≥20 and the proteins with -10logP≥20 containing at least 1 unique peptide were filtered.

Split luciferase complementation assay

The CDS of *AtALKBH9B*, *ECT2*, *UBP1B*, and *PAB2* were amplified by PCR and cloned into the modified pCAMBIA_nLUC and pCAMBIA_cLUC vectors containing the 35S promoter (primers are listed in Table S3). The constructs were transformed into the *Agrobacterium tumefaciens* strain GV3101 and then infiltrated into *Nicotiana benthamiana* leaves along with P19. The detached leaves were sprayed with 1 mM luciferin (GLPBio) at 2 days after infiltration. The luminescence signal was visualized with a Tanon-5200 (Tanon).

Fluorescence polarization

The Gag region of *Onsen* was PCR-amplified using the primers listed in Table S3, cloned into pET28a generating 6xHis-Gag and transformed into *E. coli* strain Rosetta. Starter culture was grown overnight in 4 mL LB media containing 50 μg/mL Kanamycin and 25 μg/mL Chloramphenicol at 37 ºC with shaking at 200 RPM. 3 mL of starter culture was transferred to 300 mL of LB media. Cells were grown at 37 ºC with shaking at 200 RPM until the OD600 reach between 0.6 and 0.8. The growth temperature was then lowered to

12 ºC and IPTG was added to a final concentration of 0.5 mM. Cells were incubated for two days at 12 ºC with shaking at 180 RPM and harvested by centrifugation. The pellet was resuspended in 30 mL of lysis buffer [20 mM Tris-HCl (pH 7.6), 200 mM NaCl , 10% Glycerol, 0.1% Tween20]. 60 µL 1 U/µL DNase I, 60 µL 1 M MgSO4 and 150 µL 200 mM PMSF were added, and the cells were lysed using an SCIENTZ-IID cell homogenizer (SCIENTZ). Lysates were cleared with cell debris by centrifugation at 18,000 *g* for 1 h at 4 ºC. Cleared lysates were loaded onto a Econo-Pac® Chromatography Columns column (Bio-rad) and washed with 2 column volumes of buffer [20 mM Tris-HCl (pH 7.6), 200 mM NaCl, 10% Glycerol, 0.1% Tween20, 25 mM imidazole]. Bound protein was eluted in 2 mL of buffer [20 mM Tris-HCl (pH 7.6), 200 mM NaCl, 10% Glycerol, 0.1% Tween20, 500 mM imidazole]. Protein was concentrated using a spin concentrator (Amicon, 10K MWCO) and injected onto Superdex 200 column (GE Healthcare) equilibrated in 25 mM HEPES (pH 7.5) and 100 mM NaCl. Fractions were checked for purity by SDS-PAGE followed by Coomassie blue staining. Fluorescence polarization assay was carried out following the previously described method (*75*). Binding assays were performed in 25 mM HEPES (pH 7.5) and 100 mM NaCl including 10 nM FAM-labeled RNA oligonucleotide (GGCCAACUACGU and GGCCAm^{6}ACUACGU) in black and flat-bottom 96-well plates (BBI). Proteins were serially diluted 2-fold and the final assay volume was 25 µL per well. The signal was detected at room temperature on a BioTek Synergy Neo plate reader (BioTek). Polarization (P) was converted to anisotropy (A) using the formula A = 2P/(3-P). Data were plotted as fraction bound by setting the highest anisotropy measured to 1. Data were plotted using GraphPad Prism (version 6.0), and dissociation constants (*Kd*) were obtained by fitting the curve to a non-linear regression model.

Reverse transcription efficiency

RT efficiency assay was performed using the MEGAscript® RNAi Kit (Thermo Fischer) according to the manufacturer's instructions. In brief, the template DNA was amplified using the primers containing T7 promoter (listed in Table S3). The in vitro transcription was carried out as following; 3 µL 10X T7 Reaction Buffer, 0.5 µL ATP Solution or 0.5 µL m^{6}ATP (TriLink), 1 µL each of C/G/UTP, 1 µL T7 RNA polymerase, 2.5 µL DNA (500 ng) at 37 ℃ overnight. The template DNA was removed by adding the DNase I and incubating the mixture at 37 ℃ for 2 h. RNA was purified by the ethanol precipitation method and resuspended in 20 µL RNase-free H2O. RNA was reverse transcribed using the ReverTra Ace qPCR RT Master Mix with gDNA Remover (Toyobo) for 30 sec. Subsequently, qPCR was performed as described above. The oligonucleotide sequences are provided in Table S3.

References

1. D. Lisch, How important are transposons for plant evolution? *Nat. Rev. Genet.* **14**, 49–61 (2013).
2. C. Feschotte, Transposable elements and the evolution of regulatory networks. *Nat. Rev. Genet.* **9**, 397–405 (2008).

3. R. Rebollo, M. T. Romanish, D. L. Mager, Transposable Elements: An Abundant and Natural Source of Regulatory Sequences for Host Genes. *Annu. Rev. Genet.* **46**, 21–42 (2012).
4. V. Satheesh, W. Fan, J. Chu, J. Cho, Recent advancement of NGS technologies to detect active transposable elements in plants. *Genes Genomics*. **43**, 289–294 (2021).
5. D. Lisch, Epigenetic Regulation of Transposable Elements in Plants. *Annu. Rev. Plant Biol.* **60**, 43–66 (2009).
6. H. Zhang, Z. Lang, J. K. Zhu, Dynamics and function of DNA methylation in plants. *Nat. Rev. Mol. Cell Biol.* **19**, 489–506 (2018).
7. M. A. Matzke, R. A. Mosher, RNA-directed DNA methylation: an epigenetic pathway of increasing complexity. *Nat. Rev. Genet.* **15**, 394–408 (2014).
8. R. K. Slotkin, R. Martienssen, Transposable elements and the epigenetic regulation of the genome. *Nat. Rev. Genet.* **8**, 272–285 (2007).
9. J. A. Law, S. E. Jacobsen, Establishing, maintaining and modifying DNA methylation patterns in plants and animals. *Nat. Rev. Genet.* **11**, 204–220 (2010).
10. A. Madlung, L. Comai, The effect of stress on genome regulation and structure. *Ann. Bot.* **94**, 481–495 (2004).
11. P. Negi, A. N. Rai, P. Suprasanna, Moving through the stressed genome: Emerging regulatory roles for transposons in plant stress response. *Front. Plant Sci.* **7** (2016), doi:10.3389/fpls.2016.01448.
12. H. Ito, H. Gaubert, E. Bucher, M. Mirouze, I. Vaillant, J. Paszkowski, An siRNA pathway prevents transgenerational retrotransposition in plants subjected to stress. *Nature*. **472**, 115–119 (2011).
13. V. V. Cavrak, N. Lettner, S. Jamge, A. Kosarewicz, L. M. Bayer, O. Mittelsten Scheid, How a Retrotransposon Exploits the Plant's Heat Stress Response for Its Activation. *PLoS Genet.* **10**, e1004115 (2014).
14. W. Matsunaga, A. Kobayashi, A. Kato, H. Ito, The effects of heat induction and the siRNA biogenesis pathway on the transgenerational transposition of ONSEN, a copia-like retrotransposon in Arabidopsis thaliana. *Plant Cell Physiol.* **53**, 824–833 (2012).
15. W. Matsunaga, N. Ohama, N. Tanabe, Y. Masuta, S. Masuda, N. Mitani, K. Yamaguchi-Shinozaki, J. F. Ma, A. Kato, H. Ito, A small RNA mediated regulation of a stress-activated retrotransposon and the tissue specific transposition during the reproductive period in Arabidopsis. *Front. Plant Sci.* **6**, 1–12 (2015).
16. K. Nozawa, J. Chen, J. Jiang, S. M. Leichter, M. Yamada, T. Suzuki, F. Liu, H. Ito, X. Zhong, DNA methyltransferase CHROMOMETHYLASE3 prevents ONSEN transposon silencing under heat stress. *PLOS Genet.* **17**, e1009710 (2021).
17. S. Liu, J. Jonge, M. S. Trejo-Arellano, J. Santos-González, C. Köhler, L. Hennig, Role of H1 and DNA methylation in selective regulation of transposable elements during heat stress. *New Phytol.* **229**, 2238–2250 (2021).
18. K. D. Meyer, S. R. Jaffrey, Rethinking m6A Readers, Writers, and Erasers. *Annu. Rev. Cell Dev. Biol.* **33**, 319–342 (2017).
19. T. Pan, N6-methyl-adenosine modification in messenger and long non-coding RNA. *Trends Biochem. Sci.* **38**, 204–209 (2013).
20. I. A. Roundtree, M. E. Evans, T. Pan, C. He, Dynamic RNA Modifications in Gene Expression Regulation. *Cell*. **169**, 1187–1200 (2017).
21. H. Yue, X. Nie, Z. Yan, S. Weining, N6-methyladenosine regulatory machinery in plants: composition, function and evolution. *Plant Biotechnol. J.* **17**, 1194–1208 (2019).
22. Y. Fu, D. Dominissini, G. Rechavi, C. He, Gene expression regulation mediated through reversible m6A RNA methylation. *Nat. Rev. Genet.* **15**, 293–306 (2014).

23. Y. Yue, J. Liu, C. He, RNA N6-methyladenosine methylation in post-transcriptional gene expression regulation. *Genes Dev.* **29**, 1343–1355 (2015).
24. G. Z. Luo, A. Macqueen, G. Zheng, H. Duan, L. C. Dore, Z. Lu, J. Liu, K. Chen, G. Jia, J. Bergelson, C. He, Unique features of the m6A methylome in Arabidopsis thaliana. *Nat. Commun.* **5** (2014), doi:10.1038/ncomms6630.
25. L. Shen, Z. Liang, X. Gu, Y. Chen, Z. W. N. Teo, X. Hou, W. M. Cai, P. C. Dedon, L. Liu, H. Yu, N6-Methyladenosine RNA Modification Regulates Shoot Stem Cell Fate in Arabidopsis. *Dev. Cell*. **38**, 186–200 (2016).
26. J. Scutenaire, J. M. Deragon, V. Jean, M. Benhamed, C. Raynaud, J. J. Favory, R. Merret, C. Bousquet-Antonelli, The YTH domain protein ECT2 is an m6A reader required for normal trichome branching in arabidopsis. *Plant Cell*. **30**, 986–1005 (2018).
27. H.-C. Duan, L.-H. Wei, C. Zhang, Y. Wang, L. Chen, Z. Lu, P. R. Chen, C. He, G. Jia, ALKBH10B Is an RNA N6-Methyladenosine Demethylase Affecting Arabidopsis Floral Transition. *Plant Cell*. **29**, 2995–3011 (2017).
28. L. Arribas-Hernández, S. Bressendorff, M. H. Hansen, C. Poulsen, S. Erdmann, P. Brodersen, An m6A-YTH Module Controls Developmental Timing and Morphogenesis in Arabidopsis. *Plant Cell*. **30**, 952–967 (2018).
29. S. Zhong, H. Li, Z. Bodi, J. Button, L. Vespa, M. Herzog, R. G. Fray, MTA is an Arabidopsis messenger RNA adenosine methylase and interacts with a homolog of a sex-specific splicing factor. *Plant Cell*. **20**, 1278–1288 (2008).
30. Y. Shoaib, J. Hu, S. Manduzio, H. Kang, Alpha-ketoglutarate-dependent dioxygenase homolog 10B, an N6-methyladenosine mRNA demethylase, plays a role in salt stress and abscisic acid responses in Arabidopsis thaliana. *Physiol. Plant.* **173**, 1078–1089 (2021).
31. J. Tang, J. Yang, H. Duan, G. Jia, ALKBH10B, an mRNA m6A Demethylase, Modulates ABA Response During Seed Germination in Arabidopsis. *Front. Plant Sci.* **12** (2021).
32. T. Chelmicki, E. Roger, A. Teissandier, M. Dura, L. Bonneville, S. Rucli, F. Dossin, C. Fouassier, S. Lameiras, D. Bourc'his, m6A RNA methylation regulates the fate of endogenous retroviruses. *Nature*. **591**, 312–316 (2021).
33. J. Liu, M. Gao, J. He, K. Wu, S. Lin, L. Jin, Y. Chen, H. Liu, J. Shi, X. Wang, L. Chang, Y. Lin, Y.-L. Zhao, X. Zhang, M. Zhang, G.-Z. Luo, G. Wu, D. Pei, J. Wang, X. Bao, J. Chen, The RNA m6A reader YTHDC1 silences retrotransposons and guards ES cell identity. *Nature*. **591**, 322–326 (2021).
34. S.-Y. Hwang, H. Jung, S. Mun, S. Lee, K. Park, S. C. Baek, H. C. Moon, H. Kim, B. Kim, Y. Choi, Y.-H. Go, W. Tang, J. Choi, J. K. Choi, H.-J. Cha, H. Y. Park, P. Liang, V. N. Kim, K. Han, K. Ahn, L1 retrotransposons exploit RNA m6A modification as an evolutionary driving force. *Nat. Commun.* **12**, 880 (2021).
35. F. Xiong, R. Wang, J.-H. Lee, S. Li, S.-F. Chen, Z. Liao, L. Al Hasani, P. T. Nguyen, X. Zhu, J. Krakowiak, D.-F. Lee, L. Han, K.-L. Tsai, Y. Liu, W. Li, RNA m6A modification orchestrates a LINE-1–host interaction that facilitates retrotransposition and contributes to long gene vulnerability. *Cell Res.* **31**, 861–885 (2021).
36. D. Mielecki, D. Ł. Zugaj, A. Muszewska, J. Piwowarski, A. Chojnacka, M. Mielecki, J. Nieminuszczy, M. Grynberg, E. Grzesiuk, Novel AlkB Dioxygenases—Alternative Models for In Silico and In Vivo Studies. *PLoS One*. **7**, e30588 (2012).
37. M. Martínez-Pérez, F. Aparicio, M. P. López-Gresa, J. M. Bellés, J. A. Sánchez-Navarro, V. Pallás, Arabidopsis m6A demethylase activity modulates viral infection of a plant virus and the m6A abundance in its genomic RNAs. *Proc. Natl. Acad. Sci. U. S. A.* **114**, 10755–10760 (2017).
38. L. Wang, H. Zhuang, W. Fan, X. Zhang, H. Dong, H. Yang, J. Cho, m6A RNA methylation impairs gene expression variability and reproductive thermotolerance in Arabidopsis. *Genome Biol.* **23**, 244 (2022).

39. M. Martínez-Pérez, C. Gómez-Mena, L. Alvarado-Marchena, R. Nadi, J. L. Micol, V. Pallas, F. Aparicio, The m6A RNA Demethylase ALKBH9B Plays a Critical Role for Vascular Movement of Alfalfa Mosaic Virus in Arabidopsis. *Front. Microbiol.* **12** (2021), doi:10.3389/fmicb.2021.745576.
40. L. Alvarado-Marchena, J. Marquez-Molins, M. Martinez-Perez, F. Aparicio, V. Pallás, Mapping of Functional Subdomains in the atALKBH9B m6A-Demethylase Required for Its Binding to the Viral RNA and to the Coat Protein of Alfalfa Mosaic Virus. *Front. Plant Sci.* **12** (2021), doi:10.3389/fpls.2021.701683.
41. D. H. Sanchez, J. Paszkowski, Heat-Induced Release of Epigenetic Silencing Reveals the Concealed Role of an Imprinted Plant Gene. *PLoS Genet.* **10**, e1004806 (2014).
42. J. Cho, M. Benoit, M. Catoni, H.-G. Drost, A. Brestovitsky, M. Oosterbeek, J. Paszkowski, Sensitive detection of pre-integration intermediates of long terminal repeat retrotransposons in crop plants. *Nat. Plants*. **5**, 26–33 (2019).
43. M. Thieme, S. Lanciano, S. Balzergue, N. Daccord, M. Mirouze, E. Bucher, Inhibition of RNA polymerase II allows controlled mobilisation of retrotransposons for plant breeding. *Genome Biol.* **18**, 1–10 (2017).
44. H. Gaubert, D. H. Sanchez, H. G. Drost, J. Paszkowski, Developmental restriction of retrotransposition activated in Arabidopsis by environmental stress. *Genetics*. **207**, 813–821 (2017).
45. Z. Wang, K. Tang, D. Zhang, Y. Wan, Y. Wen, Q. Lu, L. Wang, High-throughput m6A-seq reveals RNA m6A methylation patterns in the chloroplast and mitochondria transcriptomes of Arabidopsis thaliana. *PLoS One*. **12**, 1–24 (2017).
46. P. Jenjaroenpun, T. Wongsurawat, T. D. Wadley, T. M. Wassenaar, J. Liu, Q. Dai, V. Wanchai, N. S. Akel, A. Jamshidi-Parsian, A. T. Franco, G. Boysen, M. L. Jennings, D. W. Ussery, C. He, I. Nookaew, Decoding the epitranscriptional landscape from native RNA sequences. *Nucleic Acids Res.* **49**, e7–e7 (2021).
47. H. Liu, O. Begik, M. C. Lucas, J. M. Ramirez, C. E. Mason, D. Wiener, S. Schwartz, J. S. Mattick, M. A. Smith, E. M. Novoa, Accurate detection of m6A RNA modifications in native RNA sequences. *Nat. Commun.* **10**, 4079 (2019).
48. W. Fan, J. Cho, in *Methods in Molecular Biology* (2021), pp. 171–176.
49. R. J. Ries, S. Zaccara, P. Klein, A. Olarerin-George, S. Namkoong, B. F. Pickering, D. P. Patil, H. Kwak, J. H. Lee, S. R. Jaffrey, m6A enhances the phase separation potential of mRNA. *Nature*. **571**, 424–428 (2019).
50. Y. Fu, X. Zhuang, m6A-binding YTHDF proteins promote stress granule formation. *Nat. Chem. Biol.* **16**, 955–963 (2020).
51. J. R. Wheeler, S. F. Mitchell, A. Khong, T. Matheny, R. Parker, S. Jain, The Stress Granule Transcriptome Reveals Principles of mRNA Accumulation in Stress Granules. *Mol. Cell*. **68**, 808-820.e5 (2017).
52. J. A. Riback, C. D. Katanski, J. L. Kear-Scott, E. V. Pilipenko, A. E. Rojek, T. R. Sosnick, D. A. Drummond, Stress-Triggered Phase Separation Is an Adaptive, Evolutionarily Tuned Response. *Cell*. **168**, 1028-1040.e19 (2017).
53. T. Chantarachot, J. Bailey-Serres, Polysomes, Stress Granules, and Processing Bodies: A Dynamic Triumvirate Controlling Cytoplasmic mRNA Fate and Function. *Plant Physiol.* **176**, 254–269 (2018).
54. E. Y. Kim, L. Wang, Z. Lei, H. Li, W. Fan, J. Cho, Ribosome stalling and SGS3 phase separation prime the epigenetic silencing of transposons. *Nat. Plants*. **7**, 303–309 (2021).
55. M. Kosmacz, M. Gorka, S. Schmidt, M. Luzarowski, J. C. Moreno, J. Szlachetko, E. Leniak, E. M. Sokolowska, K. Sofroni, A. Schnittger, A. Skirycz, Protein and metabolite composition of Arabidopsis stress granules. *New Phytol.* **222**, 1420–1433 (2019).

56. P. Ryvkin, Y. Y. Leung, I. M. Silverman, M. Childress, O. Valladares, I. Dragomir, B. D. Gregory, L.-S. Wang, HAMR: high-throughput annotation of modified ribonucleotides. *RNA*. **19**, 1684–1692 (2013).
57. S. A. Woodson, J. G. Muller, C. J. Burrows, S. E. Rokita, A primer extension assay for modification of guanine by Ni(ll) complexes. *Nucleic Acids Res.* **21**, 5524–5525 (1993).
58. S. J. Anderson, M. C. Kramer, S. J. Gosai, X. Yu, L. E. Vandivier, A. D. L. Nelson, Z. D. Anderson, M. A. Beilstein, R. G. Fray, E. Lyons, B. D. Gregory, N6-Methyladenosine Inhibits Local Ribonucleolytic Cleavage to Stabilize mRNAs in Arabidopsis. *Cell Rep.* **25**, 1146-1157.e3 (2018).
59. B. Slobodin, R. Han, V. Calderone, J. A. F. O. Vrielink, F. Loayza-Puch, R. Elkon, R. Agami, Transcription Impacts the Efficiency of mRNA Translation via Co-transcriptional N6-adenosine Methylation. *Cell*. **169**, 326-337.e12 (2017).
60. P. C. He, C. He, m6A RNA methylation: from mechanisms to therapeutic potential. *EMBO J.* **40**, e105977 (2021).
61. S. Ke, A. Pandya-Jones, Y. Saito, J. J. Fak, C. B. Vågbø, S. Geula, J. H. Hanna, D. L. Black, J. E. Darnell, R. B. Darnell, m6A mRNA modifications are deposited in nascent pre-mRNA and are not required for splicing but do specify cytoplasmic turnover. *Genes Dev.* . **31**, 990–1006 (2017).
62. L. Arribas-Hernández, S. Rennie, T. Köster, C. Porcelli, M. Lewinski, D. Staiger, R. Andersson, P. Brodersen, Principles of mRNA targeting via the Arabidopsis m6A-binding protein ECT2. *Elife*. **10** (2021), doi:10.7554/eLife.72375.
63. D. Dominissini, S. Moshitch-Moshkovitz, M. Salmon-Divon, N. Amariglio, G. Rechavi, Transcriptome-wide mapping of N6-methyladenosine by m6A-seq based on immunocapturing and massively parallel sequencing. *Nat. Protoc.* **8**, 176–189 (2013).
64. L. Wang, E. Y. Kim, J. Cho, in *Methods in Molecular Biology* (2021), pp. 103–110.
65. Z. Lei, E. Kim, J. Cho, Enrichment of Cytoplasmic RNA Granules from Arabidopsis Seedlings. *BIO-PROTOCOL*. **11** (2021), doi:10.21769/BioProtoc.4212.
66. J. Liu, L. Feng, X. Gu, X. Deng, Q. Qiu, Q. Li, Y. Zhang, M. Wang, Y. Deng, E. Wang, Y. He, I. Bäurle, J. Li, X. Cao, Z. He, An H3K27me3 demethylase-HSFA2 regulatory loop orchestrates transgenerational thermomemory in Arabidopsis. *Cell Res.* (2019), doi:10.1038/s41422-019-0145-8.
67. A. M. Bolger, M. Lohse, B. Usadel, Trimmomatic: a flexible trimmer for Illumina sequence data. *Bioinformatics*. **30**, 2114–2120 (2014).
68. D. Kim, B. Langmead, S. L. Salzberg, HISAT: a fast spliced aligner with low memory requirements. *Nat. Methods*. **12**, 357–60 (2015).
69. M. Pertea, G. M. Pertea, C. M. Antonescu, T.-C. Chang, J. T. Mendell, S. L. Salzberg, StringTie enables improved reconstruction of a transcriptome from RNA-seq reads. *Nat. Biotechnol.* **33**, 290–5 (2015).
70. J. T. Robinson, H. Thorvaldsdottir, W. Winckler, M. Guttman, E. S. Lander, G. Getz, J. P. Mesirov, Integrative Genomics Viewer. *Nat. Biotechnol.* **29**, 24–26 (2011).
71. Y. Zhang, T. Liu, C. A. Meyer, J. Eeckhoute, D. S. Johnson, B. E. Bernstein, C. Nusbaum, R. M. Myers, M. Brown, W. Li, X. S. Liu, Model-based Analysis of ChIP-Seq (MACS). *Genome Biol.* **9**, R137 (2008).
72. H. Li, Minimap2: pairwise alignment for nucleotide sequences. *Bioinformatics*. **34**, 3094–3100 (2018).
73. J. Gleeson, A. Leger, Y. D. J. Prawer, T. A. Lane, P. J. Harrison, W. Haerty, M. B. Clark, Accurate expression quantification from nanopore direct RNA sequencing with NanoCount. *Nucleic Acids Res.* **50**, e19–e19 (2022).

74. X. Cui, Z. Wei, L. Zhang, H. Liu, L. Sun, S.-W. Zhang, Y. Huang, J. Meng, Guitar: An R/Bioconductor Package for Gene Annotation Guided Transcriptomic Analysis of RNA-Related Genomic Features. *Biomed Res. Int.* **2016**, 1–8 (2016).
75. J. S. Harrison, E. M. Cornett, D. Goldfarb, P. A. DaRosa, Z. M. Li, F. Yan, B. M. Dickson, A. H. Guo, D. V. Cantu, L. Kaustov, P. J. Brown, C. H. Arrowsmith, D. A. Erie, M. B. Major, R. E. Klevit, K. Krajewski, B. Kuhlman, B. D. Strahl, S. B. Rothbart, Hemi-methylated DNA regulates DNA methylation inheritance through allosteric activation of H3 ubiquitylation by UHRF1. *Elife*. **5** (2016), doi:10.7554/eLife.17101.
76. L. Wang, *Zenodo*, doi:10.5281/ZENODO.7969237.

Acknowledgments
We thank the Core Facility Center of CAS Center for Excellence in Molecular Plant Sciences for technical support with confocal microscopy.

Funding:
This work was supported by the grants listed below.
Chinese Academy of Sciences Strategic Priority Research Program XDB27030209 (JC)
National Natural Science Foundation of China 31970518 (JC)
National Natural Science Foundation of China 32150610473 (JC)
National Natural Science Foundation of China 32111540256 (JC)
Natural Science Foundation of Shanghai 22ZR1469100 (JC)

Author contributions:
Conceptualization: WF, JuC
Methodology: WF, LW, ZL, HL, JiC, MY, YW
Investigation: WF, LW, ZL, HL, JiC, HW, JY, JuC
Visualization: LW, JuC
Supervision: JuC
Writing—original draft: WF, LW, JuC
Writing—review & editing: JuC

Competing interests:
Authors declare that they have no competing interests.

Data and materials availability:
All data needed to evaluate the conclusions in the paper are present in the paper and/or the Supplementary Materials. The NGS data that support the findings of this study have been deposited in SRA repository with the accession codes PRJNA873867 and summarized in Table S4. The analyses were performed using the standard codes instructed by the tools described in the Methods and the custom codes used in this study are deposited in GitHub (https://github.com/JungnamChoLab) and Zenodo (*76*).

Table of contents of SM

Fig. S4. Identification of *atalkbh9b-2* and the expression of *AtALKBH9B*.
Fig. S5. *Onsen* mRNA levels in the mutants of *AtALKBH10B*.
Fig. S6. Expression levels of a non-methylated TE transcript in *atalkbh9b-1*.
Fig. S7. AtALKBH9B interactome.
Fig. S8. Split luciferase complementation assays.
Fig. S9. Western blot for the SG-enriched proteins.
Fig. S10. SG enrichment and m^{6}A level of *CCR2*.
Fig. S11. *Onsen* RNA levels in the mutants of SG components.
Fig. S12. Confocal microscopy images of Gag-GFP transgenic plants.
Fig. S13. Reverse transcription efficiency of m^{6}A-modified RNA.
Fig. S14. Selective targeting of SG localization and AtALKBH9B-mediated demethylation.
Table S1. Oligonucleotide sequences used in this study.
Table S2. Summary of NGS data.
Table S3. List of proteins interacting with AtALKBH9B.
Table S4. List of SG-associated and AtALKBH9B-interacting proteins.

Figures and Tables

Fig. 1. *Onsen* RNA is m^{6}A-modified. (A) Distribution of m^{6}A RNA modification in 5' UTR, CDS, and 3' UTR. m^{6}A enrichment was calculated for regions spanning 1% of total length. HS, heat-stressed sample (3 h) ; CS, control sample. Data from the wt floral buds are shown. (B) Overlap of m^{6}A-containing transcripts in CS and HS. m^{6}A-modified transcripts were defined as those containing m^{6}A peaks detected by MACS2 at FDR lower than 0.05. (C) Fraction of transposons in each category presented in B. *P* values were obtained by the two-tailed Student's t-test. (D) Fraction of genes (n=15413) and transposons (n=57) with m^{6}A RNA modifications. Genes and transposons with FPKM values greater than 5 in the heat-stressed flower sample are only considered. (E) m^{6}A-RIP-seq showing an *Onsen* locus and the m^{6}A sites detected by ONT-DRS. For ONT-DRS experiment, one-week-old Col-0 seedlings treated with 24 h of heat stress at 37 °C were used for RNA extraction. Numbers in brackets indicate the range of coverage values (m^{6}A-RIP-seq) and fraction of m^{6}A RNA modification (ONT-DRS). Rep, biological replicate. (F) Volcano plot of m^{6}A enrichment. Enrichment score was determined by normalizing the m^{6}A levels to input levels. The red dots are individual *Onsen* copies and *AT1TE12295* is marked. (G) Validation of m^{6}A enrichment by qPCR. RNA was extracted from the wt seedlings heat-stressed for 24 h. Regions tested are as indicated in E. *Act2* was used as an internal control. Data are shown in mean ± s.d. from three biological replications. *P* values were obtained from the comparison to region A by the two-tailed Student's t-test.

Fig. 2. *AtALKBH9B* regulates *Onsen* by directly binding to its transcripts. (A) Gene structure of *AtALKBH9B*. T-DNA insertion of *atalkbh9b-1* is shown as a triangle. The *atalkbh9b-2* mutant contains a large deletion of 65 bp in the first exon. Grey and black boxes indicate UTRs and exons, respectively. (B) *Onsen* RNA levels in the *atalkbh9b* mutants determined by RT-qPCR. One-week-old seedlings treated with 24 h of heat stress at 37 °C were used for RNA extraction. *Act2* was used as an internal control. Data are shown in mean ± s.d. from three biological replications. *P* values were obtained by the two-tailed Student's t-test. (C) RNA-seq of *atalkbh9b-1* showing the *Onsen* locus. Numbers in brackets indicate the

range of coverage values. Rep, biological replicate. Arrowheads are primers used in B, D, and F. (D) RT-qPCR for complementation assay of the *atalkbh9b-1* mutant with the *pAtALKBH9B::AtALKBH9B-GFP* construct. *Act2* was used as an internal control. Data are shown in mean ± s.d. from three biological replications. *P* values were obtained by the two-tailed Student's t-test. (E) m^6A-RIP-qPCR performed in the heat-stressed wt, *atalkbh9b-1* mutant, and a mutant complementing line. Regions are as indicated in Fig. 1E. *Act2* was used as an internal control. Data are shown in mean ± s.d. from three biological replications. *P* values were obtained by the two-tailed Student's t-test. (F) RIP-qPCR experiments using the *pAtALKBH9B::AtALKBH9B-GFP* transgenic plants used in D. RNA was extracted from seedlings heat-stressed from 24 h. Immunoprecipitation was performed using an anti-GFP antibody. Data are shown in mean ± s.d. from three biological replications. *P* values were obtained by the two-tailed Student's t-test.

Fig. 3. Retrotransposition activity of *Onsen* is reduced in *atalkbh9b-1*. (A and B) EclDNA (A) and total DNA (B) levels of *Onsen* in the *atalkbh9b-1* mutant. Amplification of linear extrachromosomal DNA (ALE)-qPCR was performed to determine the eclDNA levels. DNA was extracted from seedlings subjected to control and 24 h-heat stress treatment. In A, PCR-amplified *Evade* DNA was used as a spike-in control and in B, *Act2* was used as an internal control. CS, control sample; HS, heat-stressed sample. Data are shown in mean ± s.d. from three biological replications. *P* values were obtained by the two-tailed Student's t-test. (C and D) Copy number of *Onsen* in the progenies of wt (n=20) and *atalkbh9b-1* (n=19) (C) and *nrpd1a-3* (n=10) and *nrpd1a-3 atalkbh9b-1* double mutant (n=10) (D) that were subjected to heat stress treatment. Copy number was determined by droplet digital PCR using *CBF2* as a single-copy reference gene. *P* values were obtained by the two-sided Mann-Whitney U test.

Fig. 4. AtALKBH9B is localized to stress granules upon heat. (A) Co-localization of AtALKBH9B-GFP and SGS3-TdTomato tested in tobacco transient expression system. CS, control sample; HS, heat-stressed for 12 h. Bar=20 μm. (B and C) Co-localization of AtALKBH9B-GFP and SGS3-TdTomato in *Arabidopsis* double transgenic plants subjected to heat stress for 12 h (B). Root epidermal cells of heat-stressed plants are shown. Arrow indicates the section for which the signal intensity was quantitated (C). Bar=10 μm. (D) Interactome of AtALKBH9B revealed by IP/MS. Heat-stressed *pUBQ10::AtALKBH9B-GFP* transgenic *Arabidopsis* plants were used. Proteins are color-coded by their functional categories. Edges with darker color represent stronger protein-protein interactions. The IP/MS experiment was performed with three independent biological replicates. Proteins with the $-10\log_{10}P$ values greater than 20 were filtered, and those involved in RNA regulation were chosen for visualization. (E) Interaction of AtALKBH9B and ECT2 determined by a split luciferase assay performed in tobacco transient expression system.

Fig. 5. SG enrichment of m^6A-modified RNA. (A) RNA dot blot analysis of m^6A RNA modification in the total and SG-enriched RNA. Total and SG RNA derived from

the 24 h-heat stressed *atalkbh9b-1* mutant plants were used. (B) Signal intensity of the blot shown in A is quantitated. Values are mean ± s.d. from three biological replications. (C) Number of m^6A peaks in the total and SG-enriched transcripts. SG enrichment score is defined as the log_2-transformed fold change of SG to total RNA levels. SG-enriched transcripts are those with SG enrichment score greater than 1. (D) m^6A levels of the SG-enriched transcripts detected by ONT-DRS. m^6A level of a transcript was determined by the mean fraction of m^6A RNA modification from all detected m^6A sites by ONT-DRS. Transcripts with FPKM values greater than 10 are only considered. SG-enriched transcripts are those with SG enrichment score greater than 0.5 (n=194). *P* values were obtained by the one-sided Wilcoxon rank sum text. (E-G) In E, cumulative distribution for the SG enrichment of the transcripts upregulated in *atalkbh9b-1* (FC>=1, n=217) as compared with the randomly selected transcripts (n=217). In F, SG enrichment of the transcripts hypermethylated in *atalkbh9b-1* (Δm^6A>=0.2, n=165). In G, SG enrichment score is compared between wt and *atalkbh9b-1*. *P* values were obtained by the one-sided Wilcoxon rank sum text. (H) SG enrichment of *Onsen* RNA in the *atalkbh9b-1* mutant determined by qPCR. Normalization was against total RNA. *CCR2* was used as a negative control which is strongly marked by m^6A but is not regulated by AtALKBH9B (fig. S10). Data are shown in mean ± s.d. from three biological replications. *P* values were obtained by the two-tailed Student's t-test.

Fig. 6. m^6A RNA methylation inhibits binding of Gag in vitro and in vivo. (A) Fluorescence polarization assay of purified Gag protein encoded by *Onsen*. 12-mer RNA oligos with or without m^6A modification (GGCCAACUACGU and GGCCAm^6ACUACGU) were used. Data are shown in mean ± s.d. from four technical replications. *P* values were obtained by the two-way ANOVA. (B) RIP-qPCR of Gag-GFP binding to *Onsen* transcript. The *OnsenLTR::Gag-GFP* construct was introgressed to *atalkbh9b-1* by genetic cross. Regions tested are as described in Fig. 1E. Data are shown in mean ± s.d. from three biological replications. *P* values were obtained by the two-tailed Student's t-test.

Fig. 7. A proposed model. m^6A-modified *Onsen* RNA is localized to SG. AtALKBH9B demethylates and releases *Onsen* RNA out of SG. Demethylated *Onsen* RNA assembles to VLP by interacting with Gag and is reverse transcribed to form eclDNA. In the mutant of *AtALKBH9B*, *Onsen* RNA is hypermethylated and localized in SG. In addition, RNA methylation inhibits the binding of Gag and reverse transcription. Closed and open circles represent m^6A-methylated and unmethylated sites, respectively; dashed line indicates nuclear envelop; wavy single line is RNA and wavy double line is DNA.

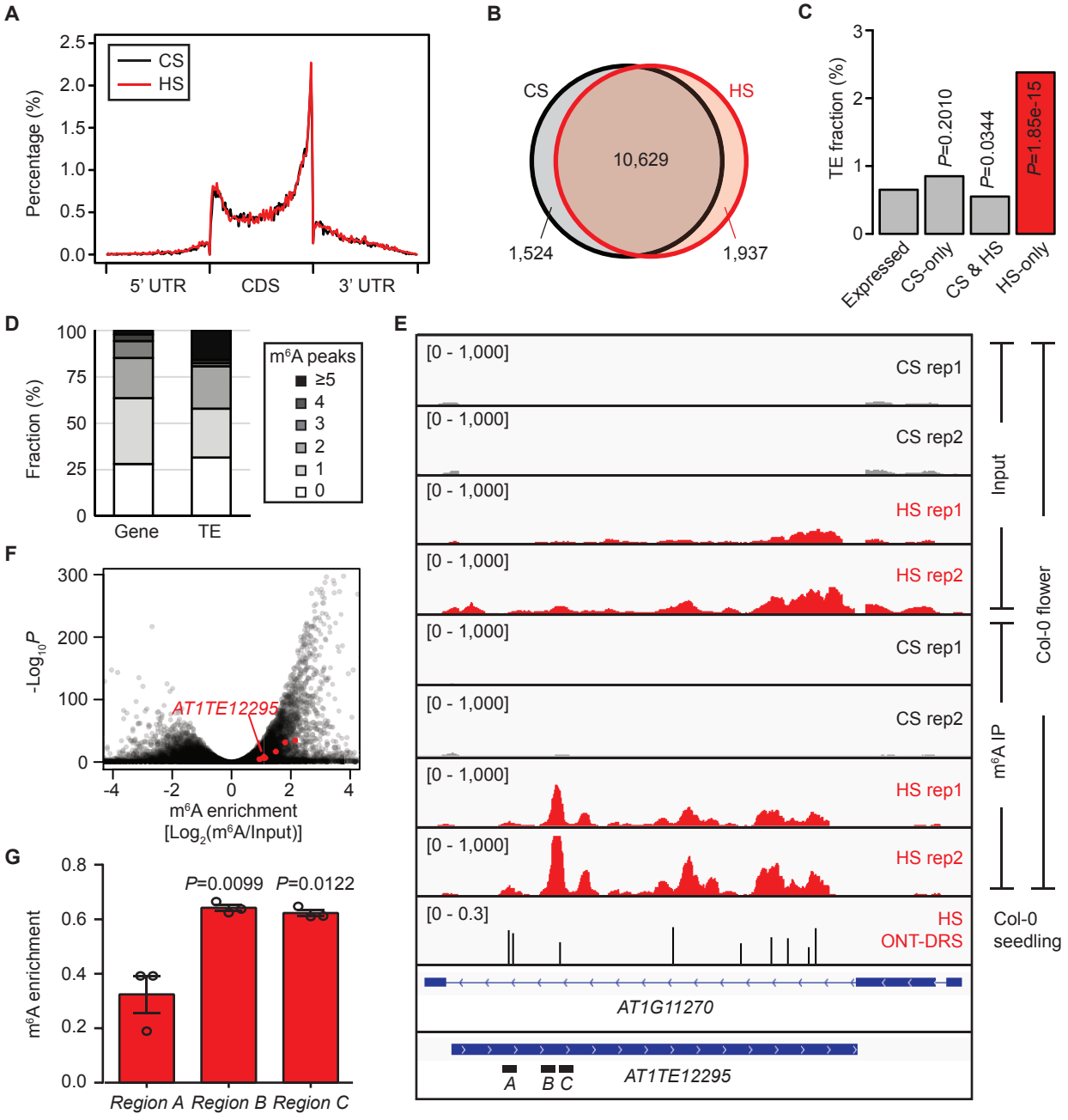
A
Percentage (%)
CS
HS
5' UTR
CDS
3' UTR
B
CS
HS
10,629
1,524
1,937
C
TE fraction (%)
P=0.2010
P=0.0344
P=1.85e-15
Expressed
CS-only
CS & HS
HS-only
D
Fraction (%)
m6A peaks
≥5
4
3
2
1
0
Gene
TE
E
[0 - 1,000]
CS rep1
CS rep2
HS rep1
HS rep2
[0 - 0.3]
HS
ONT-DRS
Input
m6A IP
Col-0 flower
Col-0
seedling
AT1G11270
AT1TE12295
A
B C
F
-Log10P
AT1TE12295
m6A enrichment
[Log2(m6A/Input)]
G
m6A enrichment
P=0.0099
P=0.0122
Region A
Region B
Region C

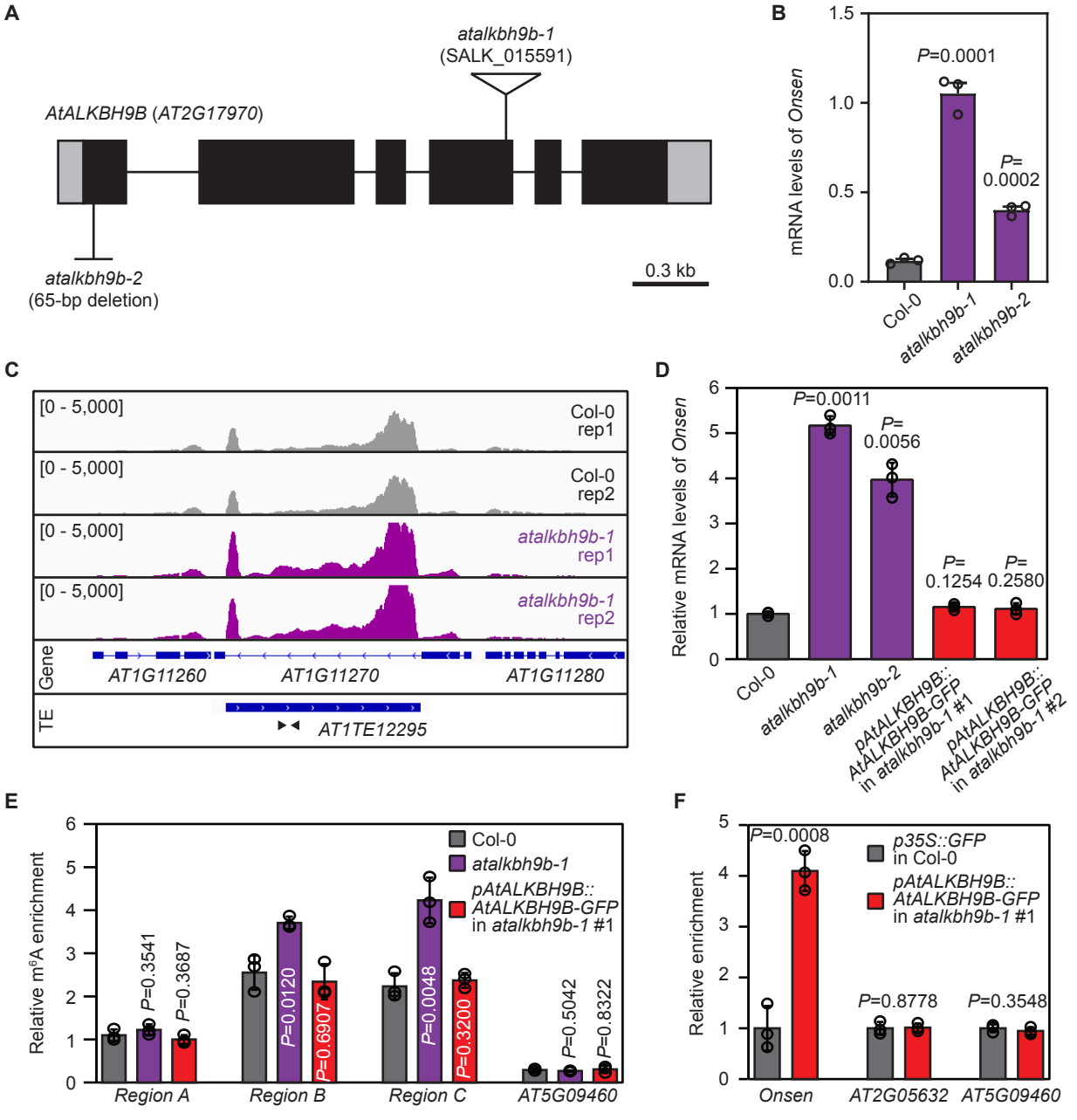
A
atalkbh9b-1
(SALK_015591)
AtALKBH9B (AT2G17970)
atalkbh9b-2
(65-bp deletion)
0.3 kb
B
mRNA levels of Onsen
P=0.0001
P=
0.0002
Col-0
atalkbh9b-1
atalkbh9b-2
C
[0 - 5,000]
Col-0
rep1
Col-0
rep2
atalkbh9b-1
rep1
atalkbh9b-1
rep2
Gene
AT1G11260
AT1G11270
AT1G11280
TE
AT1TE12295
D
Relative mRNA levels of Onsen
P=0.0011
P=
0.0056
P=
0.1254
P=
0.2580
Col-0
atalkbh9b-1
atalkbh9b-2
pAtALKBH9B::
AtALKBH9B-GFP
in atalkbh9b-1 #1
pAtALKBH9B::
AtALKBH9B-GFP
in atalkbh9b-1 #2
E
Relative m6A enrichment
Col-0
atalkbh9b-1
pAtALKBH9B::
AtALKBH9B-GFP
in atalkbh9b-1 #1
P=0.3541
P=0.3687
P=0.0120
P=0.6907
P=0.0048
P=0.3200
P=0.5042
P=0.8322
Region A
Region B
Region C
AT5G09460
F
Relative enrichment
P=0.0008
p35S::GFP
in Col-0
pAtALKBH9B::
AtALKBH9B-GFP
in atalkbh9b-1 #1
P=0.8778
P=0.3548
Onsen
AT2G05632
AT5G09460

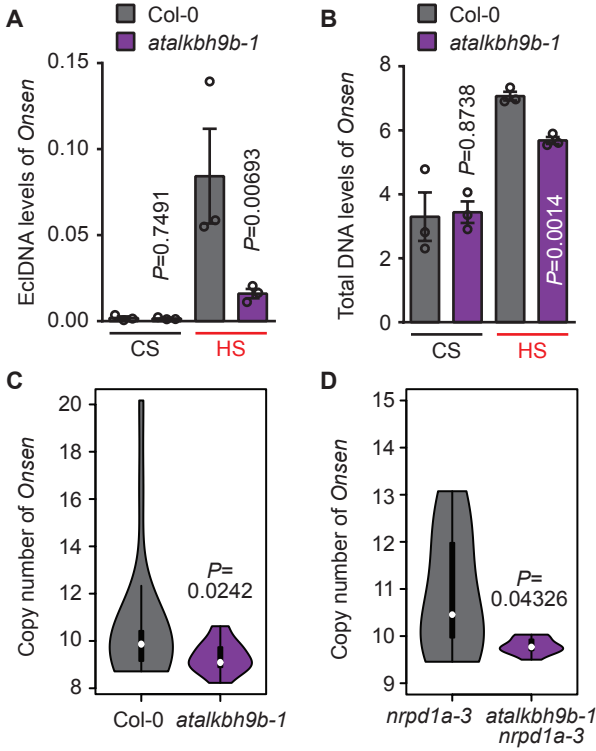
A
Col-0
atalkbh9b-1
EcIDNA levels of Onsen
0.15
0.10
0.05
0.00
P=0.7491
P=0.00693
CS
HS
B
Col-0
atalkbh9b-1
Total DNA levels of Onsen
8
6
4
2
0
P=0.8738
P=0.0014
CS
HS
C
Copy number of Onsen
20
18
16
14
12
10
8
P=
0.0242
Col-0
atalkbh9b-1
D
Copy number of Onsen
15
14
13
12
11
10
9
P=
0.04326
nrpd1a-3
atalkbh9b-1
nrpd1a-3

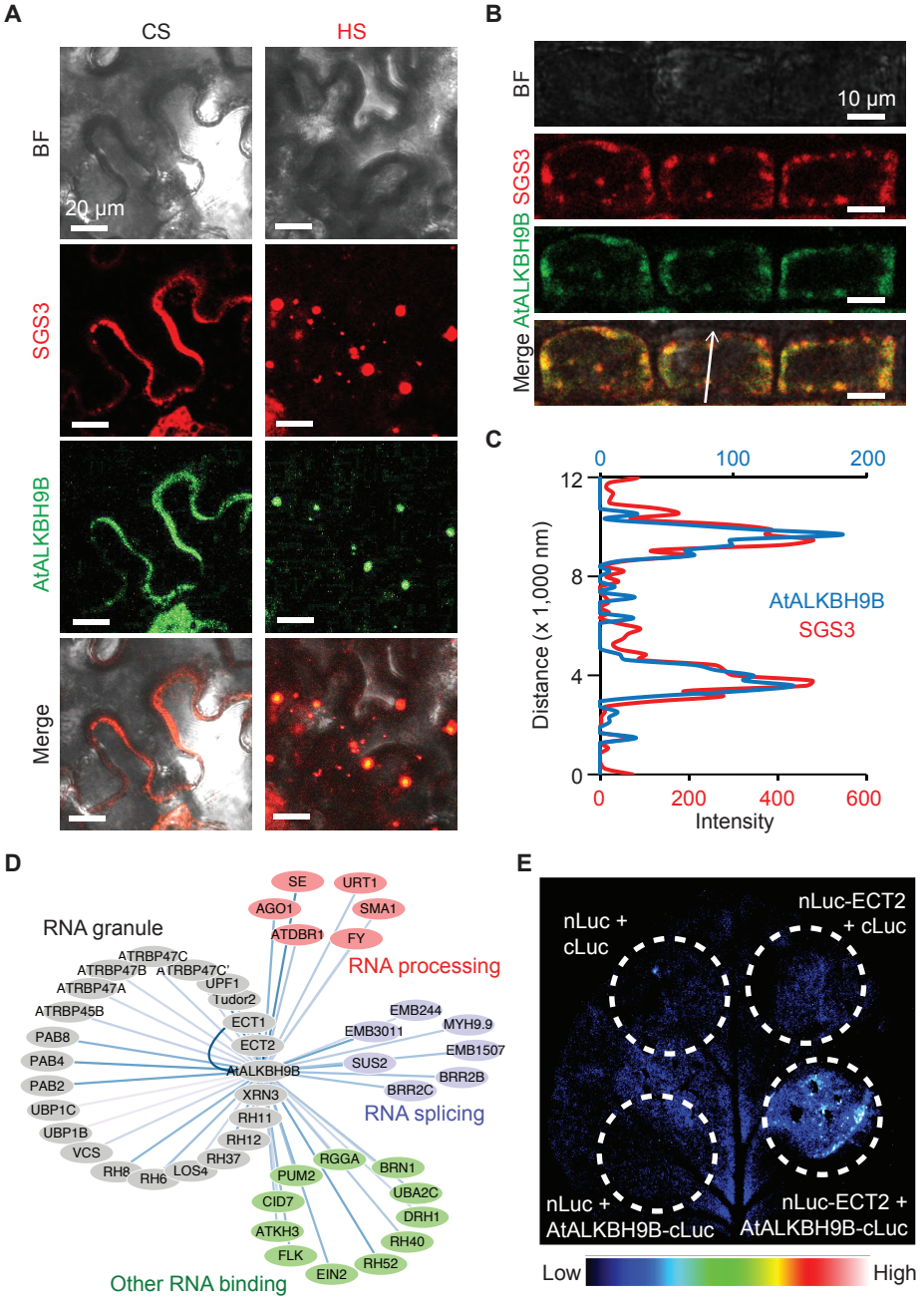
A
CS
HS
BF
SGS3
AtALKBH9B
Merge
20 μm
B
BF
10 μm
SGS3
AtALKBH9B
Merge
C
0
100
200
12
8
4
0
Distance (x 1,000 nm)
AtALKBH9B
SGS3
0
200
400
600
Intensity
D
RNA granule
RNA processing
RNA splicing
Other RNA binding
SE
URT1
AGO1
SMA1
ATDBR1
FY
ATRBP47C
ATRBP47B
ATRBP47C'
ATRBP47A
UPF1
Tudor2
ATRBP45B
ECT1
ECT2
PAB8
PAB4
PAB2
AtALKBH9B
UBP1C
UBP1B
VCS
RH8
RH6
LOS4
RH37
RH12
RH11
XRN3
EMB244
MYH9.9
EMB3011
EMB1507
SUS2
BRR2B
BRR2C
RGGA
BRN1
PUM2
UBA2C
CID7
DRH1
ATKH3
RH40
FLK
RH52
EIN2
E
nLuc +
cLuc
nLuc-ECT2
+ cLuc
nLuc +
AtALKBH9B-cLuc
nLuc-ECT2 +
AtALKBH9B-cLuc
Low
High

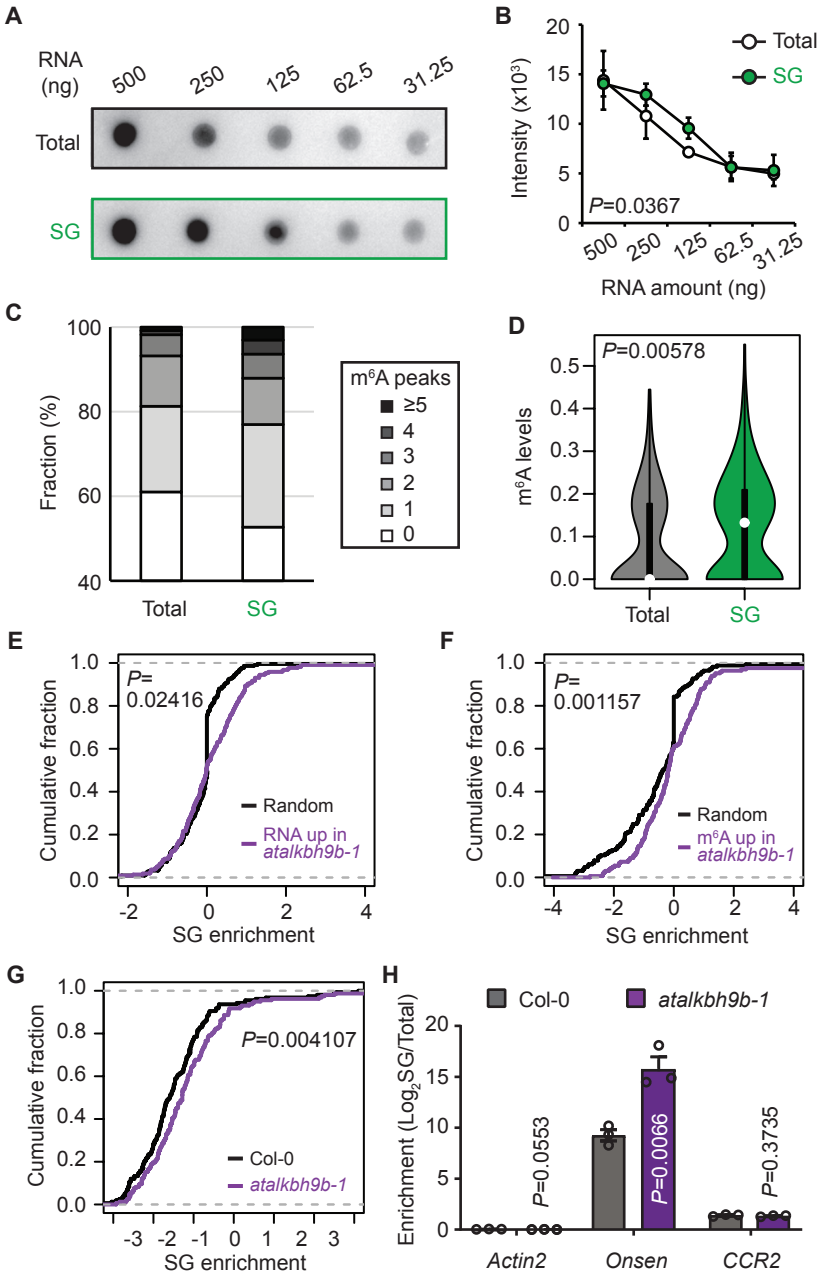
A
RNA (ng)
500
250
125
62.5
31.25
Total
SG
B
Intensity (x10³)
Total
SG
P=0.0367
RNA amount (ng)
C
Fraction (%)
m⁶A peaks
≥5
4
3
2
1
0
Total
SG
D
P=0.00578
m⁶A levels
Total
SG
E
P= 0.02416
Cumulative fraction
Random
RNA up in atalkbh9b-1
SG enrichment
F
P= 0.001157
Cumulative fraction
Random
m⁶A up in atalkbh9b-1
SG enrichment
G
P=0.004107
Cumulative fraction
Col-0
atalkbh9b-1
SG enrichment
H
Col-0
atalkbh9b-1
Enrichment (Log2SG/Total)
P=0.0553
P=0.0066
P=0.3735
Actin2
Onsen
CCR2

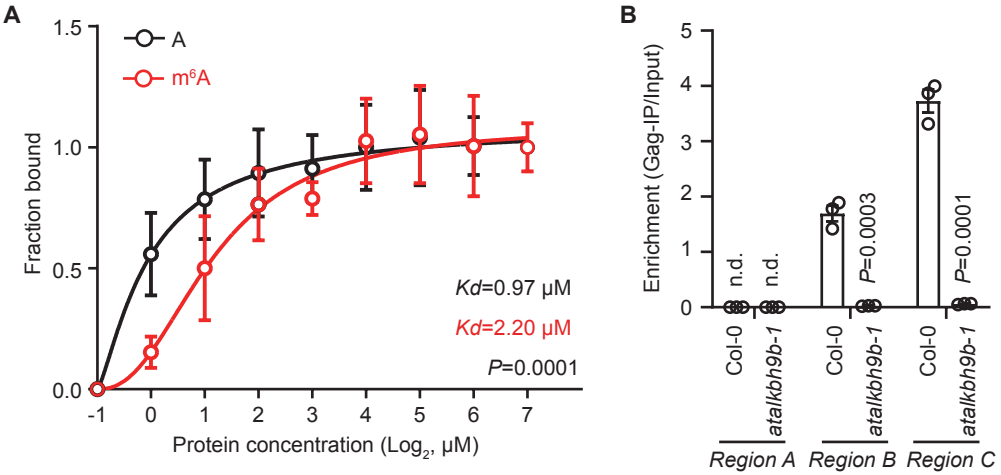
A
1.5
1.0
0.5
0.0
A
m6A
Fraction bound
Kd=0.97 μM
Kd=2.20 μM
P=0.0001
-1
0
1
2
3
4
5
6
7
Protein concentration (Log2, μM)
B
5
4
3
2
1
0
Enrichment (Gag-IP/Input)
n.d.
n.d.
P=0.0003
P=0.0001
Col-0
atalkbh9b-1
Col-0
atalkbh9b-1
Col-0
atalkbh9b-1
Region A
Region B
Region C

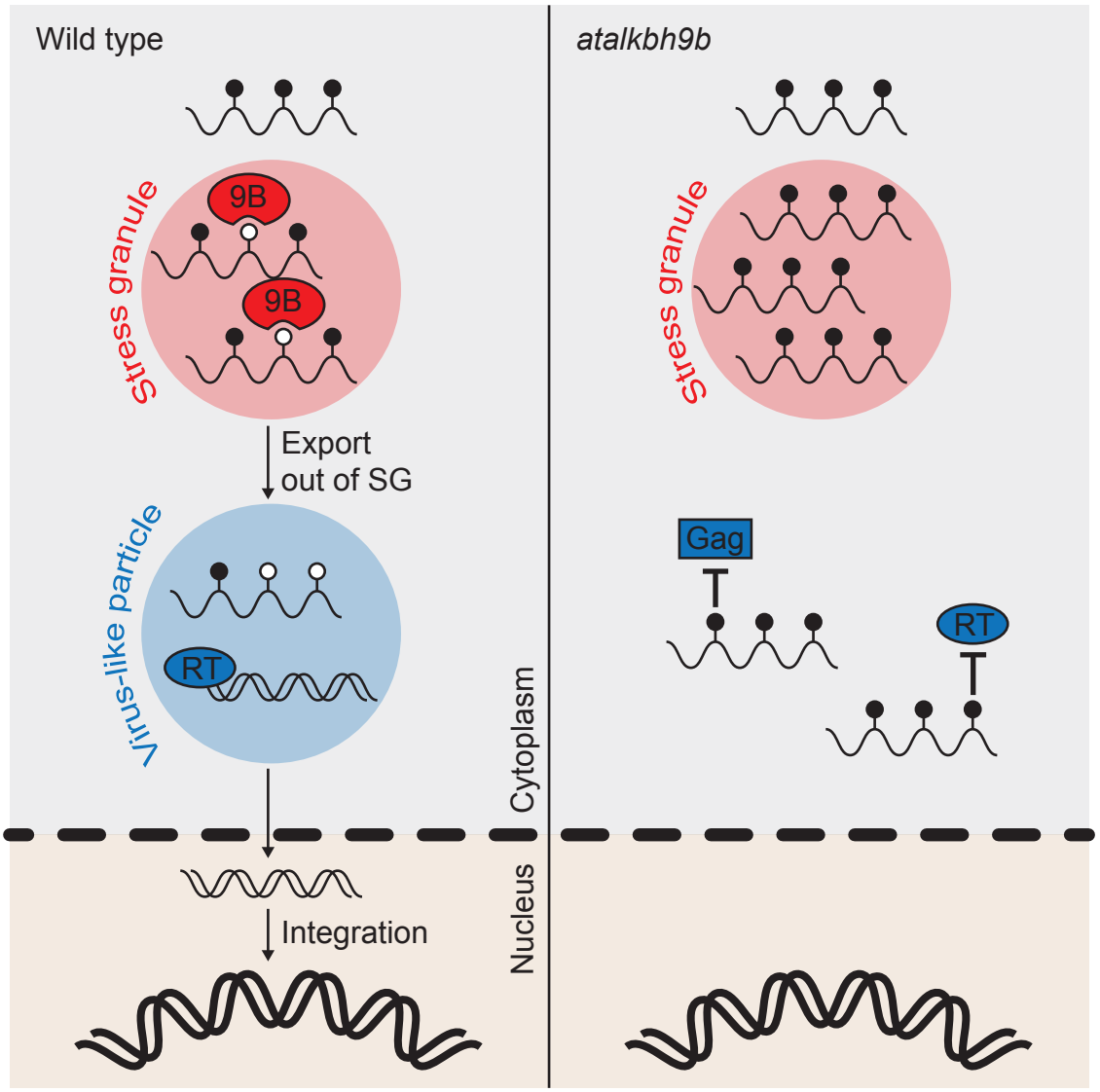
Wild type
atalkbh9b
Stress granule
9B
9B
Export
out of SG
Virus-like particle
RT
Cytoplasm
Nucleus
Integration
Stress granule
Gag
RT

Science Advances
AAAS

Supplementary Materials for

m^{6}A RNA demethylase AtALKBH9B promotes mobilization of a heat-activated long terminal repeat retrotransposon in *Arabidopsis*

Wenwen Fan *et al.*

*Corresponding author. Email: jungnam.cho@durham.ac.uk

This PDF file includes:

Figs. S1 to S14
Tables S1 to S4
Supplementary Excel File

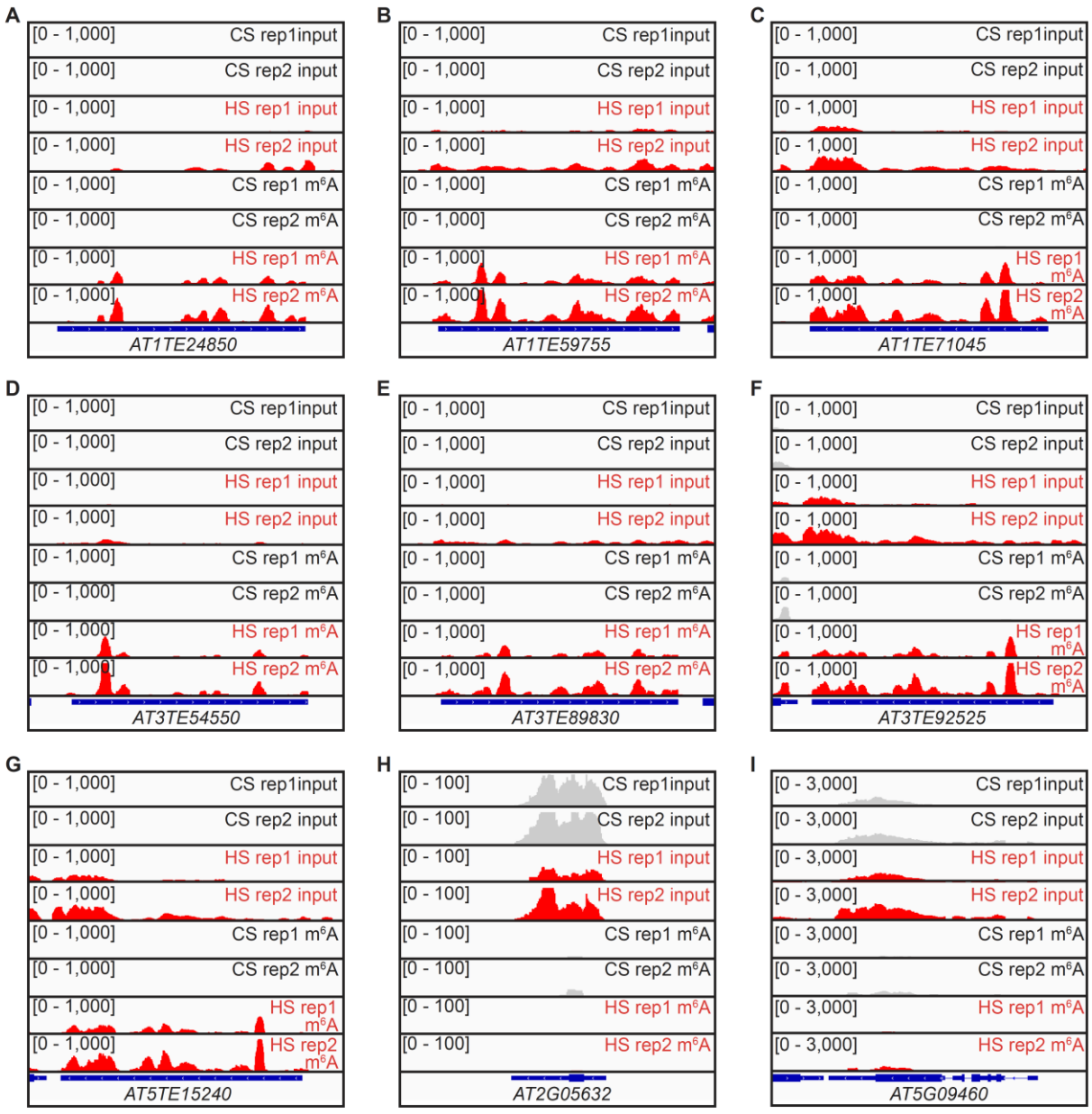

Fig. S1. m^{6}A RNA modification of *Onsen* retroelements.

Genome browser snapshots of the m^{6}A-RIP-seq data for *Onsen* retroelements (A-G) and negative control loci with low m^{6}A levels (H and I). Y axis represents the read coverage, and the coverage range is indicated in parentheses. CS, control sample; HS, heat-stressed sample; rep, biological replicates.

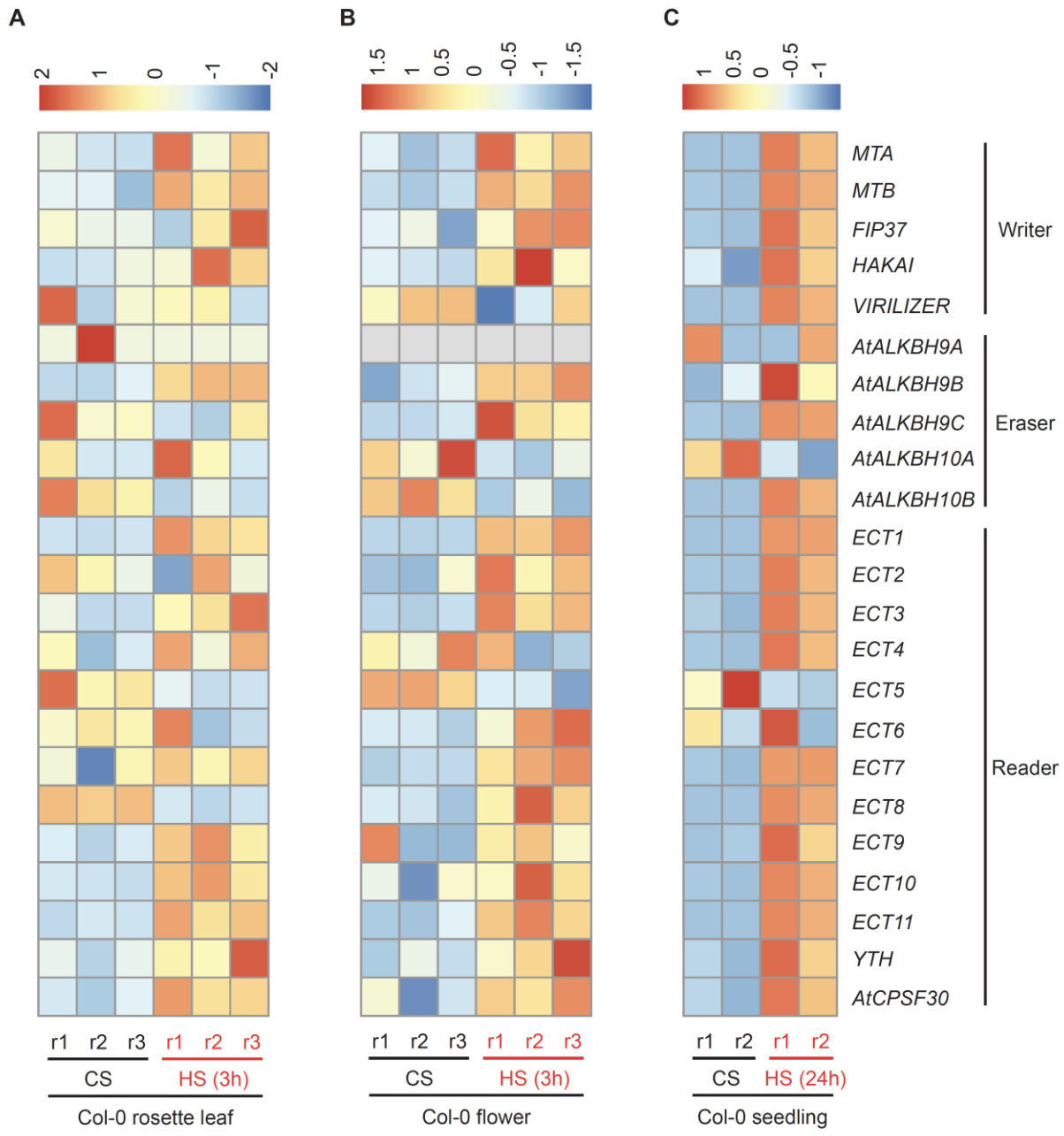

Fig. S2. Heat responsiveness of m^{6}A-related factors.

(A-C) Heatmap displaying the expression profiles of m^{6}A regulators in *Arabidopsis* wt leaves (A), flowers (B) and seedlings (C) in the control and heat stress condition. RNA-seq datasets were obtained from the studies of Wang et al. (*38*) and Gaubert et al. (*44*). r, biological repetitions; CS, control sample; HS, heat-stressed sample.

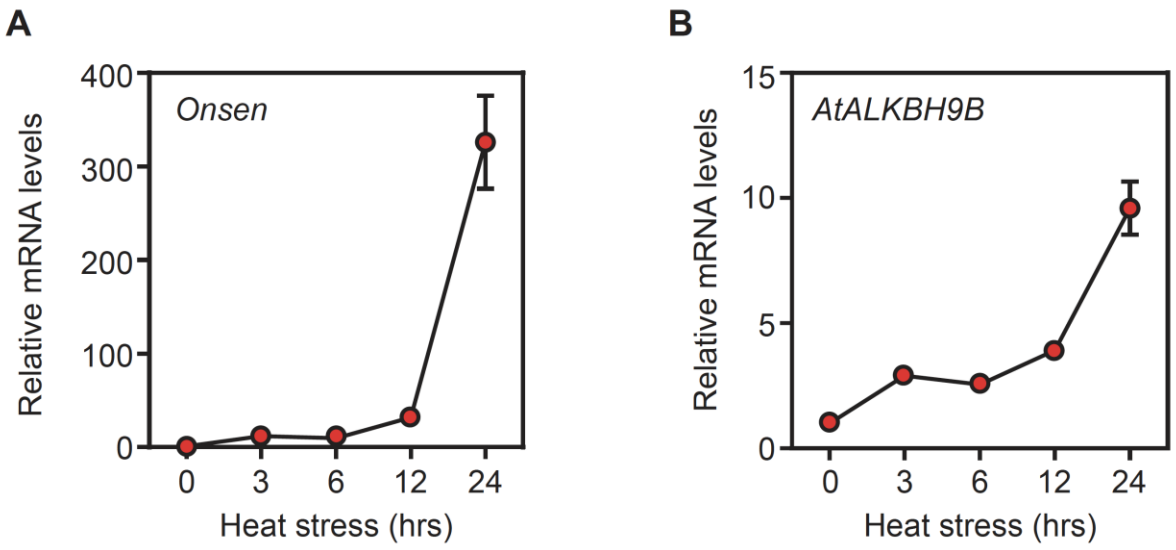

Fig. S3. Gene expression kinetics of *Onsen* and *AtALKBH9B* upon heat.

(A and B) RT-qPCR assays for the expression pattern of *Onsen* (A) and *AtALKBH9B* (B) in various duration of the heat stress treatment. Data are shown in mean ± s.d. from three biological replications and normalization is against *Act2*.

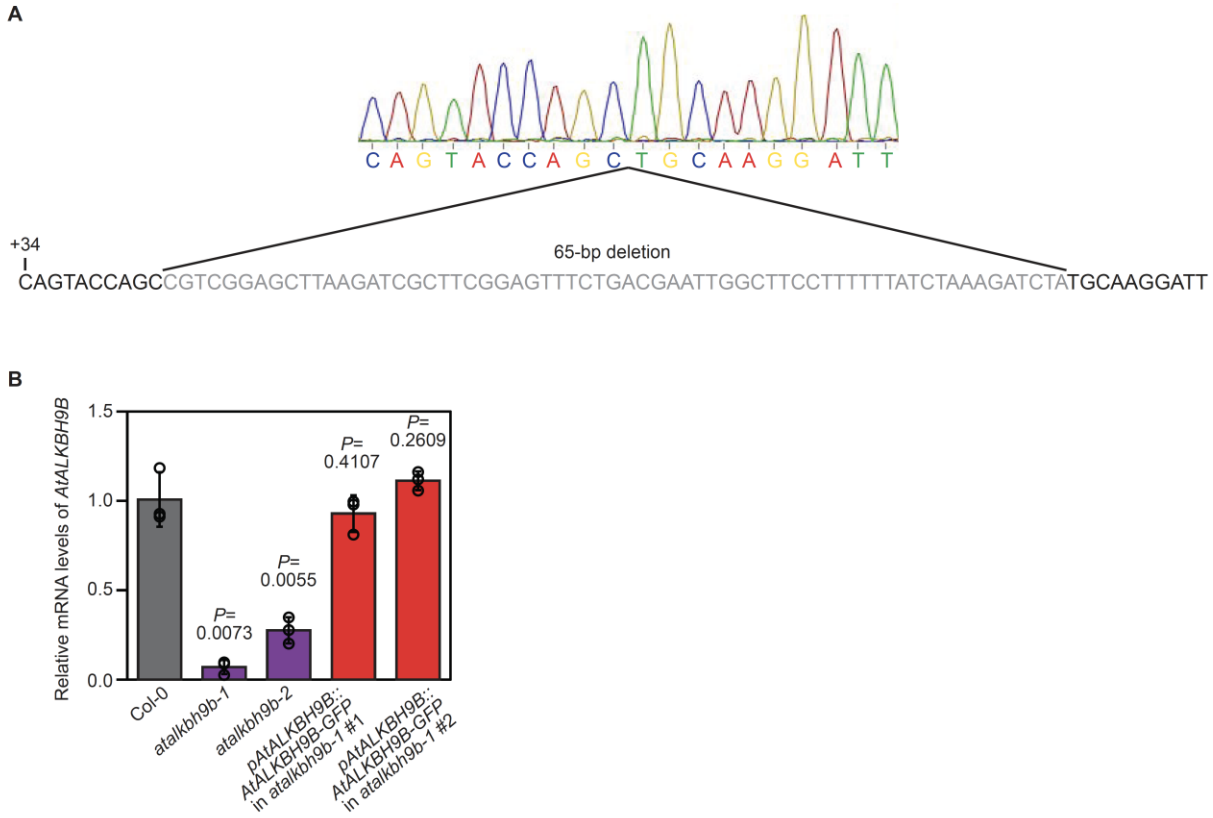

Fig. S4. Identification of *atalkbh9b-2* and the expression of *AtALKBH9B*.

(A) Chromatogram of Sanger sequencing results for the *atalkbh9b-2* mutant. *Arabidopsis* plants transformed with the CRISPR-Cas9 construct were screened at T2 generation. (B) RT-qPCR for the *AtALKBH9B* expression levels in the wt, two *atalkbh9b* mutants and two independent complementing lines. *Act2* was used as an internal control. Data are shown in mean ± s.d. from three biological replications. *P* values were obtained by the two-tailed Student's t-test.

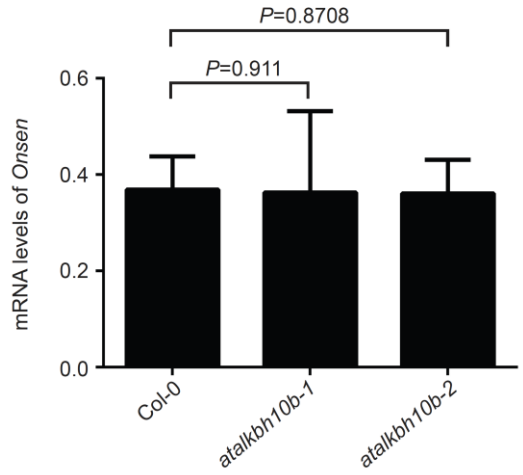

Fig. S5. *Onsen* mRNA levels in the mutants of *AtALKBH10B*.

Expression levels of *Onsen* in the *atalkbh10b-1* and *atalkbh10b-2* mutants determined by RT-qPCR. Plants were heat-stressed at 37 °C for 24 h and harvested for RNA extraction immediately after the heat treatment. *Act2* was used as an internal control. Data are shown in mean ± s.d. from three biological replications. *P* values were obtained by the two-tailed Student's t-test.

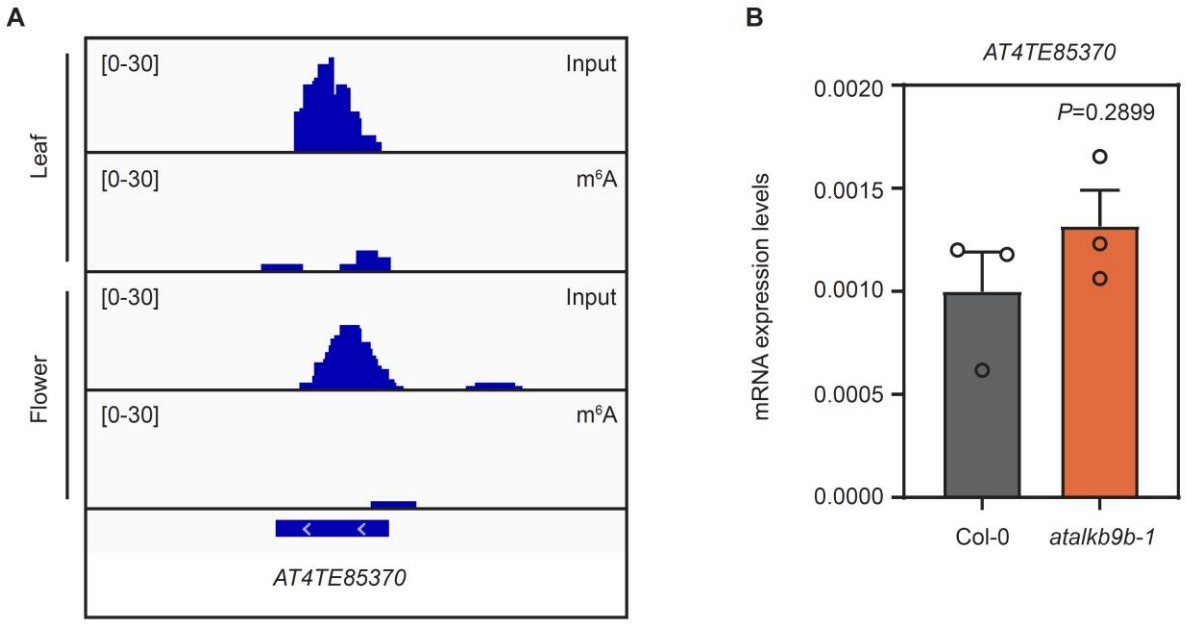

Fig. S6. Expression levels of a non-methylated TE transcript in *atalkbh9b-1*.

(A) A genome browser snapshot for m^{6}A-RIP-seq showing the AT4TE85370 locus in the heat-stressed wt leaf and flower samples. Y axis is the coverage of sequenced reads. (B) RT-qPCR for AT4TE85370 in the heat-stressed Col-0 and *atalkbh9b-1* mutant. *Act2* was used as an internal control. Data are shown in mean ± s.d. from three biological replications. *P* values were obtained by the two-tailed Student's t-test.

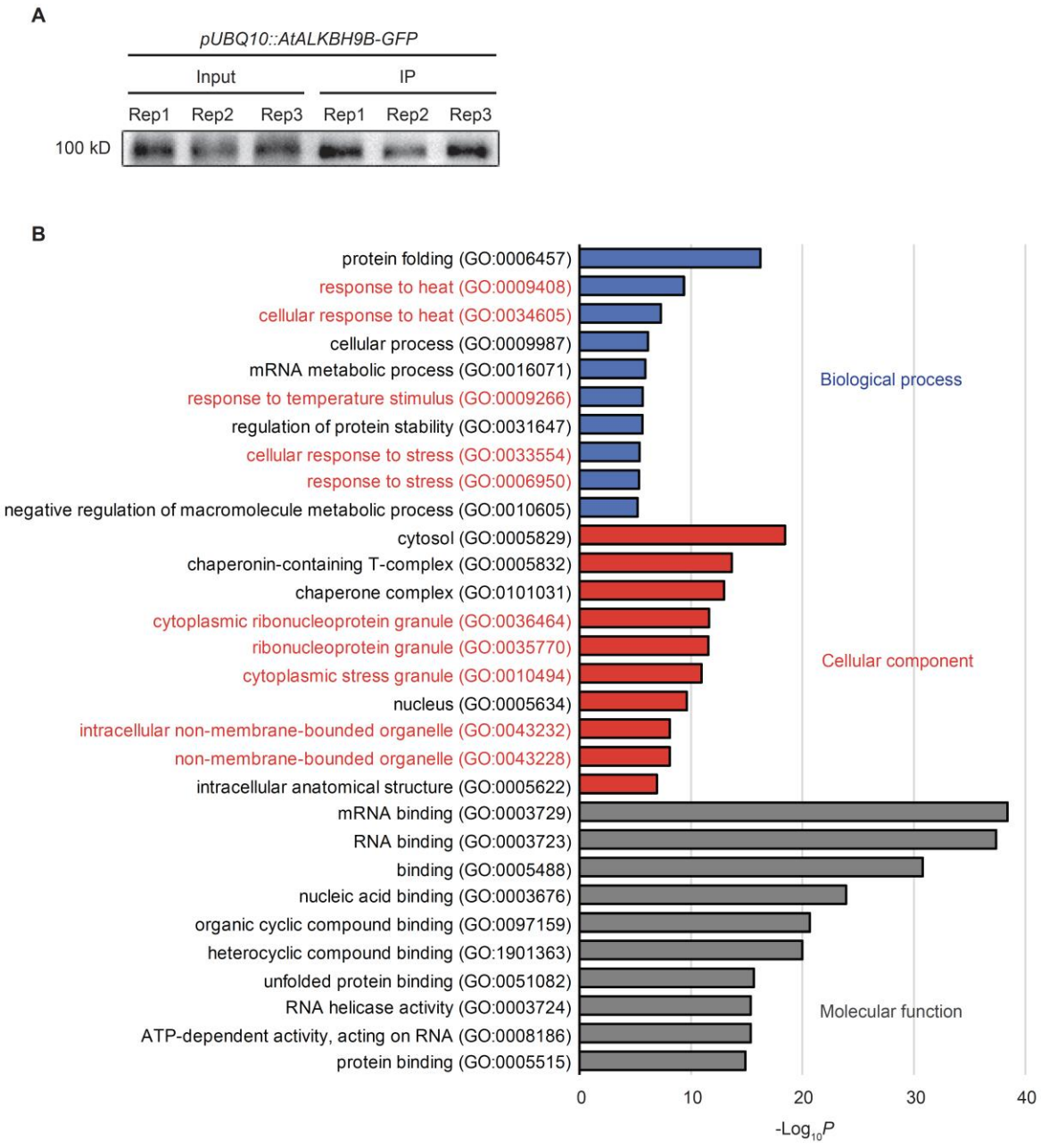

Fig. S7. AtALKBH9B interactome.

(A) Western blot image showing the AtALKBH9B-GFP proteins in the input and immunoprecipitated samples. (B) Gene enrichment analysis of the proteins identified by the IP/MS experiment using the *pUBQ10::AtALKBH9B-GFP* transgenic plants.

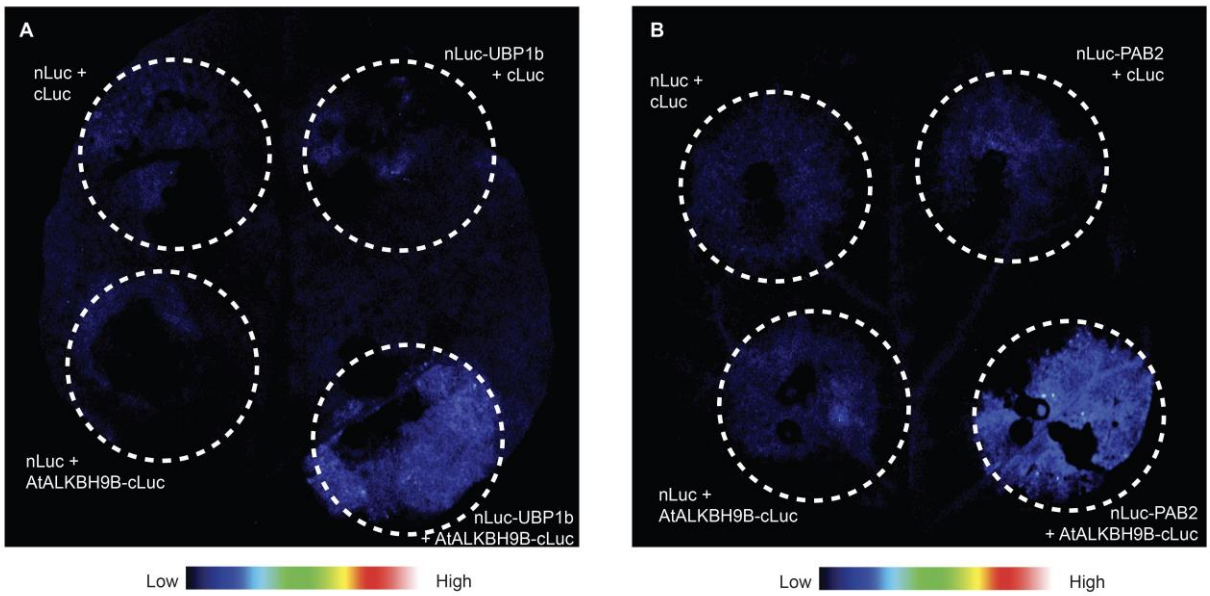

Fig. S8. Split luciferase complementation assays.

(A and B) Protein-protein interactions assessed by the split luciferase assays between AtALKBH9B and UBP1b (**a**), and AtALKBH9B and PAB2 (**b**).

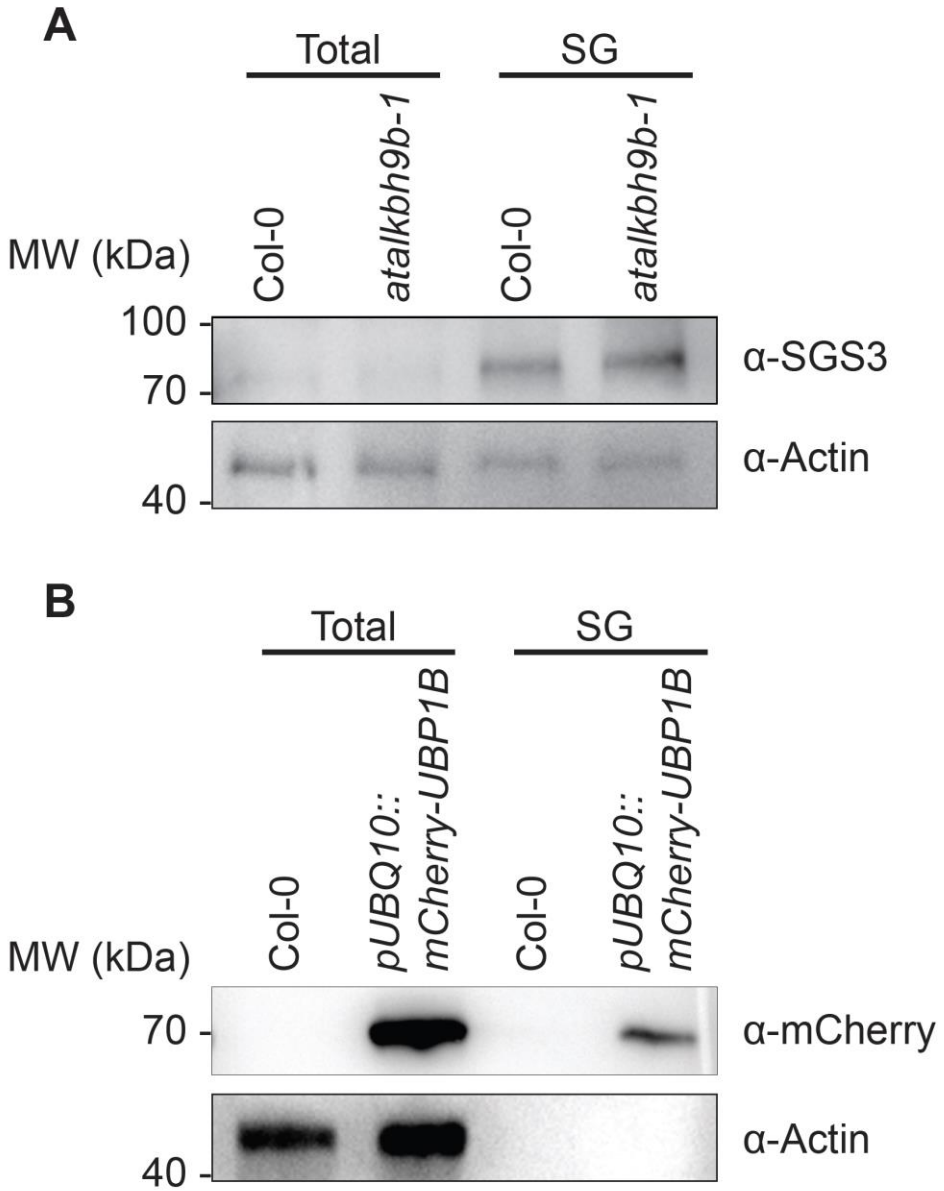

Fig. S9. Western blot for the SG-enriched proteins.

(A and B) Proteins were extracted from the heat-stressed wt and *atalkbh9b-1* (A), and the heat-stressed wt and *pUBQ10::mCherry-UBP1b* (B) before and after SG enrichment. Plants were grown in normal condition for 1 week and treated with heat stress at 37 °C for 24 hrs.

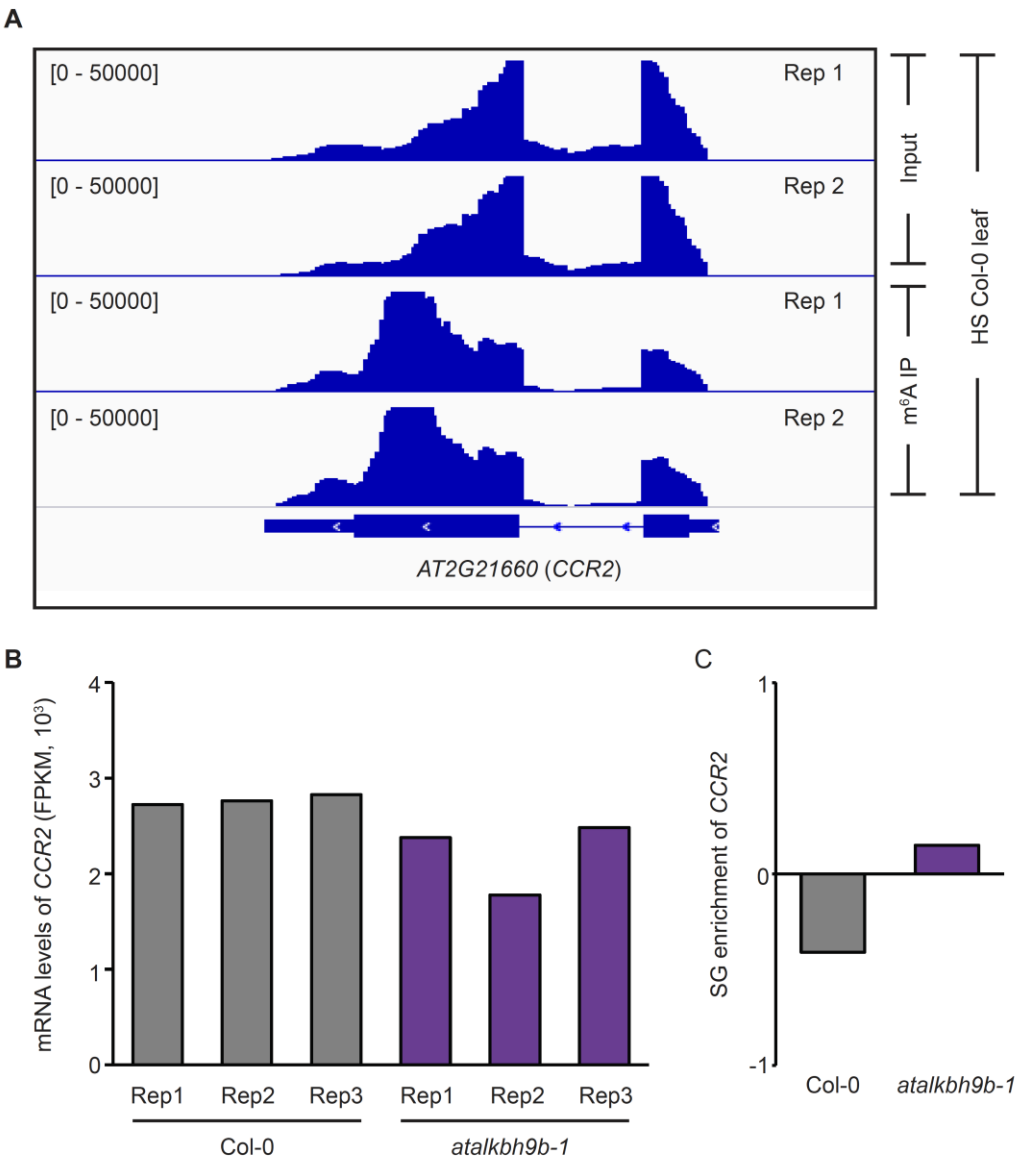

Fig. S10. SG enrichment and m^{6}A level of *CCR2*.

(A) A genome browser snapshot for m^{6}A-RIP-seq showing the *CCR2* locus in the heat-stressed wt leaf sample. Y axis is the coverage of sequenced reads. (B) The mRNA levels of *CCR2* in the heat-stressed wt and *atalkbh9b-1* mutants assessed by RNA-seq. (C) The SG enrichment score of *CCR2* in the wt and *atalkbh9b-1* mutants. SG enrichment score was determined by the $\log_2$-transformed fold change of SG to total RNA levels.

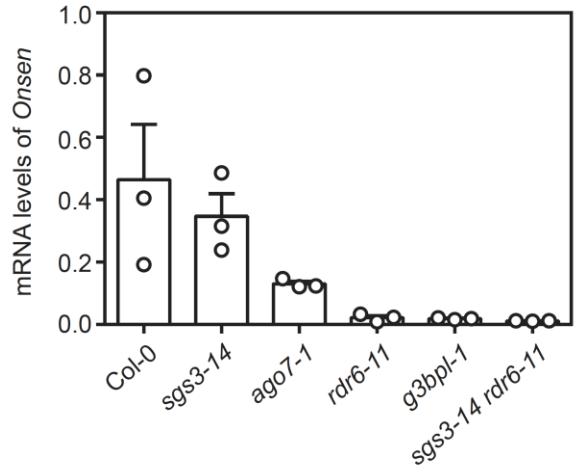

Fig. S11. *Onsen* RNA levels in the mutants of SG components.

Levels of *Onsen* RNA determined by RT-qPCR. Plants were heat-stressed for 24 h at 37 °C and harvested immediately after the heat treatment. *Act2* was used as an internal control. Data are shown in mean ± s.d. from three biological replications.

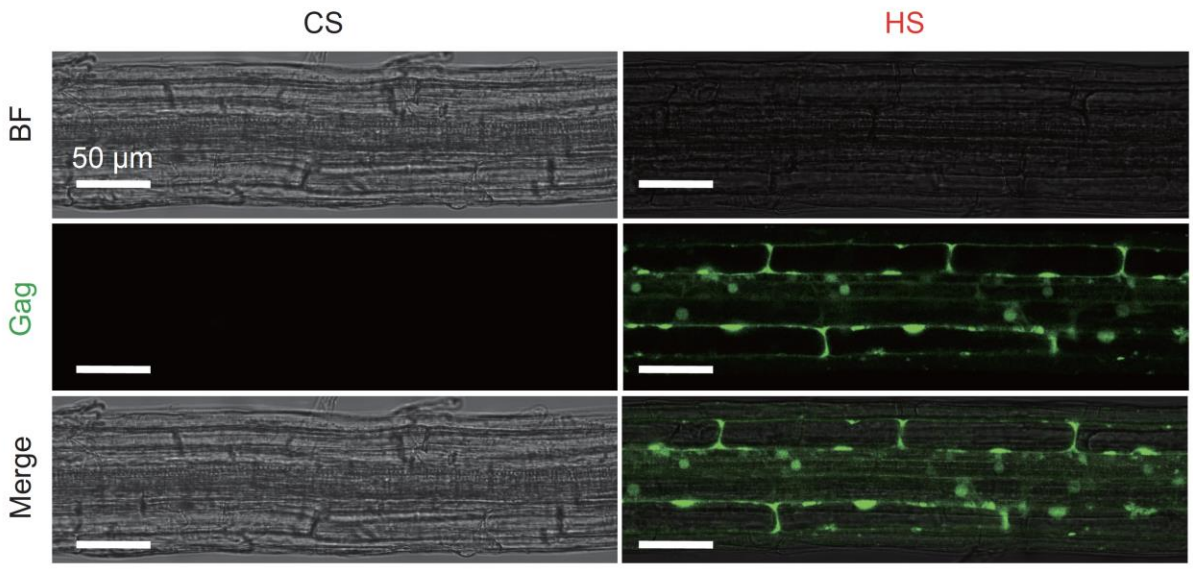

Fig. S12. Confocal microscopy images of Gag-GFP transgenic plants.

Representative confocal microscopy images of *Arabidopsis* transgenic plants expressing the *OnsenLTR::Gag-GFP* construct. Plants were tested for green fluorescence in the control (CS) and heat stress (HS) conditions with pre-heating for 12 h at 37 °C before microscopy imaging. Bar=50 µm.

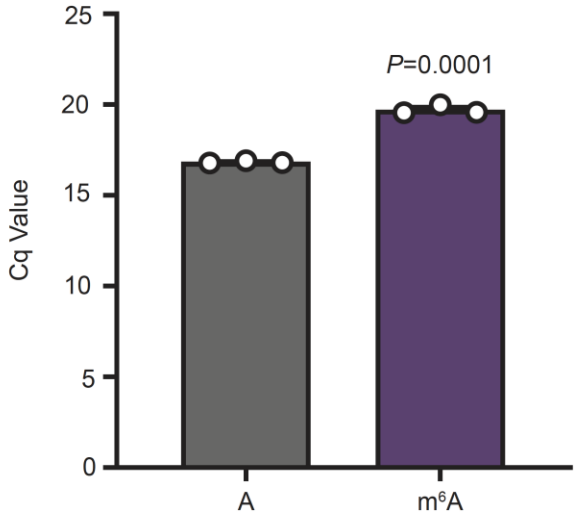

Fig. S13. Reverse transcription efficiency of m^{6}A-modified RNA.

RT-qPCR experiments using the in vitro transcribed *Onsen* RNAs that are either unmodified or m^{6}A-modified. Values are mean ± s.d. from three biological replications. *P* values were obtained by the two-tailed Student's t test.

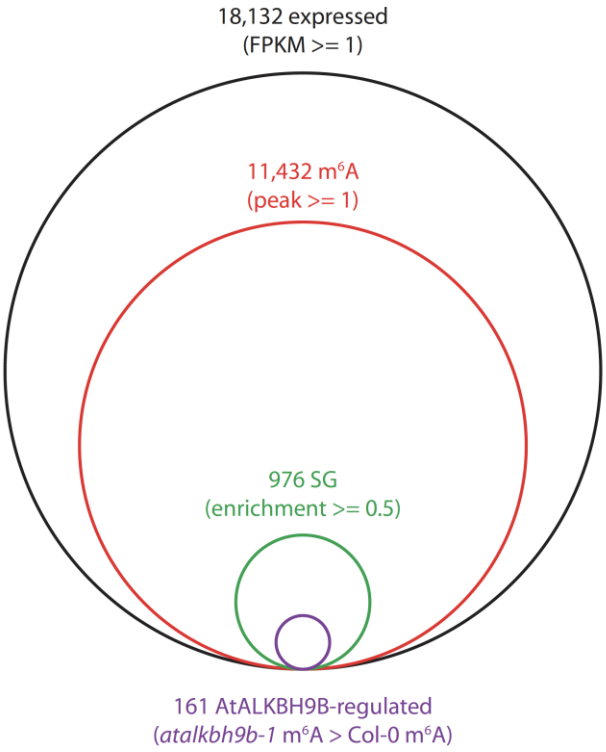

Fig. S14. Selective targeting of SG localization and AtALKBH9B-mediated demethylation. Number of transcripts with diverse features as indicated. The cut-off values for selection are provided.

Gene id	*GFP*	*AtALKBH9B-GFP* rep1	*AtALKBH9B-GFP* rep2	*AtALKBH9B-GFP* rep3	$-10\log_{10}P$
AT1G02500	2	13	12	14	211.88
AT1G07360	0	8	7	13	167.37
AT1G10170	1	24	29	24	240.89
AT1G10200	0	2	1	1	44.25
AT1G11650	0	2	1	2	73.33
AT1G16030	14	38	48	40	286.83
AT1G17370	0	1	1	1	31.65
AT1G20960	1	6	5	3	100.15
AT1G24510	0	6	8	7	145.9
AT1G29250	0	5	4	3	90.97
AT1G30070	0	1	3	1	37.43
AT1G33680	0	5	3	5	94.35
AT1G43850	0	4	1	3	87.7
AT1G45201	0	5	3	6	113.09
AT1G47490	0	3	2	2	73.11
AT1G47500	0	3	2	2	73.11
AT1G48410	0	5	5	6	130.34
AT1G49600	0	2	1	2	60.73
AT1G49760	1	3	4	7	132.33
AT1G66260	0	6	5	9	135.56
AT1G72150	0	4	5	5	134.83
AT1G72610	0	1	5	2	85.91
AT1G75560	0	4	0	5	114.23
AT1G75660	1	8	7	5	134.07
AT1G76010	1	7	9	8	162.02
AT1G79920	5	20	22	27	209.82
AT1G80070	0	7	9	8	141.95
AT1G80410	0	1	3	5	107.86
AT2G02160	0	2	3	1	117.01
AT2G17870	0	4	2	3	133.26
AT2G17970	0	228	212	221	442
AT2G18510	0	1	1	1	61.89
AT2G20190	0	10	7	11	203.08
AT2G21130	0	1	1	1	38.82
AT2G23350	3	10	10	9	184.24
AT2G26150	0	5	5	5	113.08
AT2G26280	0	2	3	1	58.3
AT2G27100	1	14	9	13	243.15
AT2G29190	0	3	2	3	97.59
AT2G32120	2	7	6	5	142.87
AT2G32700	0	5	4	3	179.59
AT2G33730	0	2	1	2	75.81
AT2G36880	3	15	12	16	222.41

AT2G42270	0	8	7	3	104.6
AT2G42520	0	9	6	8	181.9
AT2G45620	0	2	2	2	84.65
AT2G45810	0	3	2	3	110.49
AT3G01090	0	6	5	5	119.38
AT3G01540	0	1	0	3	65.65
AT3G02530	0	12	7	11	178.44
AT3G03060	0	1	2	2	81.59
AT3G03950	0	4	4	2	138.52
AT3G03960	0	6	6	4	162.61
AT3G04590	0	2	1	3	88.66
AT3G04610	1	5	3	4	119.78
AT3G06410	0	1	1	1	40.4
AT3G06480	0	2	1	3	90.17
AT3G09440	9	37	28	34	263.77
AT3G09840	0	1	1	1	61.78
AT3G11830	0	8	11	5	186.7
AT3G11910	0	5	6	5	143.48
AT3G12050	0	2	1	3	102.44
AT3G12130	1	5	3	5	116.02
AT3G13300	0	1	2	0	62.62
AT3G13460	0	3	2	3	101.76
AT3G14100	0	1	1	1	31.65
AT3G15010	0	2	2	3	93.95
AT3G16420	0	1	3	1	99.97
AT3G17390	2	17	14	17	223.21
AT3G18190	0	7	10	5	155.74
AT3G19130	0	2	1	2	60.73
AT3G20050	0	4	9	8	168.79
AT3G23300	0	4	3	1	91.15
AT3G27700	0	1	1	1	46.67
AT3G29160	0	3	1	2	81.65
AT3G50670	1	3	3	8	116.09
AT3G53110	0	2	1	1	60.76
AT3G53520	0	1	2	5	103.76
AT3G54470	0	3	3	1	116.26
AT3G58510	0	10	10	11	196.36
AT3G58570	0	6	5	6	150.37
AT3G59350	0	4	2	4	104.45
AT3G61240	0	5	3	5	143.97
AT3G62830	0	1	4	3	118.15
AT4G00660	0	7	1	6	125.2
AT4G01850	1	12	9	13	207.11
AT4G03110	0	2	2	1	48.56
AT4G08350	0	6	1	1	86.62

AT4G09150	1	12	14	14	153.65
AT4G14360	0	3	2	2	89.1
AT4G16830	0	4	1	1	62.74
AT4G23650	0	1	1	2	81.17
AT4G27320	1	3	4	5	138.14
AT4G31770	0	4	1	1	95.52
AT4G34110	2	6	7	9	160.5
AT4G34660	0	2	2	3	98.14
AT4G38130	0	2	1	1	58.01
AT4G38740	0	1	1	1	38.82
AT5G02530	0	9	7	10	161.84
AT5G03280	0	2	3	3	124.39
AT5G03340	0	1	1	1	61.78
AT5G06600	0	9	10	7	167.11
AT5G08450	0	5	4	4	106
AT5G09880	0	2	1	1	83.23
AT5G13010	0	9	7	7	156.81
AT5G13480	0	1	1	1	73.84
AT5G16070	0	9	5	8	182.67
AT5G18550	0	1	1	1	40.4
AT5G20890	0	4	3	3	151.33
AT5G26360	0	3	4	3	105.5
AT5G28540	3	13	13	18	209.42
AT5G36230	0	1	1	1	47.06
AT5G37720	0	14	10	11	179.44
AT5G42950	0	11	8	14	204.62
AT5G47010	0	23	12	22	245.26
AT5G52640	5	22	17	19	255.25
AT5G54430	0	3	3	3	111.43
AT5G56010	4	28	26	22	261.92
AT5G56030	4	28	26	22	260.7
AT5G59950	0	5	4	3	89.5
AT5G61140	0	5	4	2	103.45
AT5G61780	0	5	3	4	107.34
AT5G62090	0	2	1	1	72.4
AT5G65250	0	1	2	1	59.33
AT5G65410	0	1	1	1	42

Table S1. List of proteins interacting with AtALKBH9B.

Number of peptides and *P* values are shown for AtALKBH9B-GFP IP/MS experiments.

Gene id	*GFP*	*AtALKBH9B: GFP* rep1	*AtALKBH9B: GFP* rep2	*AtALKBH9B: GFP* rep3	$-10\log_{10}P$
AT1G24510	0	6	8	7	145.9
AT2G42520	0	9	6	8	181.9
AT3G09440	9	37	28	34	263.77
AT3G14100	0	1	1	1	31.65
AT3G58510	0	10	10	11	196.36
AT5G20890	0	4	3	3	151.33
AT3G13460	0	3	2	3	101.76
AT4G34110	2	6	7	9	160.5
AT2G23350	3	10	10	9	184.24
AT1G49760	1	3	4	7	132.33
AT1G11650	0	2	1	2	73.33
AT3G19130	0	2	1	2	60.73
AT4G38740	0	1	1	1	38.82
AT5G61780	0	5	3	4	107.34
AT3G13300	0	1	2	0	62.62

Table S2. List of SG-associated and AtALKBH9B-interacting proteins.

SG-associated proteins were identified in a previous study by Kosmacz et al. (*55*). Number of peptides and *P* values are shown.

Primer name	Sequence（5’ to 3’）
Genotype	
*atalkbh9b-1*_genotyping-F	CGAGTTCGATGAAGACTCCAG
*atalkbh9b-1*_genotyping-R	ATCCTGTTGAATAGAACCGGG
*atalkbh9b-2*_genotyping-F	AGAATTTTAAACGGCCCAAGAG
*atalkbh9b-2*_genotyping-R	AGCTCTTTCTGATCCCATATTTTCC
*atalkbh10b-1*_genotyping-F	TCCCTCTCATCACCAACAAAG
*atalkbh10b-1*_genotyping-R	ATGCCATAGCCATGAAGATTG
*atalkbh10b-2*_genotyping-F	AGTAGAAAACACATGCCTCGG
*atalkbh10b-2*_genotyping-R	TTAACATCGAGCCAATTCCAC
*ago7-1*_genotyping-F	GTATTCTGGAGGCAGAGGAGC
*ago7-1*_genotyping-R	CTCCTCCTTTTCTTTTGCACC
*sgs3-14*_genotyping-F	AAATTTGGAGTCCAGAATCGG
*sgs3-14*_genotyping-R	CAAAGCATCGGAATCATTCTC
*g3bpl-1*_genotyping-F	AAATGACAAGACCGGATCATG
*g3bpl-1*_genotyping-R	TATCAAGTGTTGCAGCAGCAG
*Cas9*_genotyping-F	TCCACACCTGAAGCGTTGATAG
*Cas9*_genotyping-R	ATGGATAAGAAGTACTCTATCGGACT
*eGFP*_genotyping-F	GTGAACCGCATCGAGCTGAA
*eGFP*_genotyping-R	ACGTTGTGGCTGTTGTAGTTG
*TdTomato*_genotyping-F	TAATGCAGAAGAAGACCATGGGC
*TdTomato*_genotyping-R	GGAAGGACAGCTTCTTGTAATC
SALK_LB1.3	ATTTTGCCGATTTCGGAAC
Cloning	
AtALKBH9B promoter_EcoRI-F	CGCGAATTCTGTGGTGTGGTGTGGTGTG
AtALKBH9B promoter_SacI-R	CGGGAGCTCGAGATACGCTCGATACAATCCAAA
AtALKBH9B gDNA_SacI-F	CGGGAGCTCATGGAAAACGATCCATTTCTCCG
AtALKBH9B gDNA_KpnI-R	TGCGGTACCACCGTAGTTTCTTCTACTAGGACG
*eGFP*_XbaI-F	TGCTCTAGAATGGTGAGCAAGGGCGAG
*eGFP*_PstI-R	CGCCTGCAGCTTGTACAGCTCGTCCATGC
*HSP18.2*_PstI-F	CGCCTGCAGTGAATATGAAGATGAAGATGAAATATTT
*HSP18.2*_HindIII-R	CGCAAGCTTCTTATCTTTAATCATATTCCATA
Onsen LTR_HindIII-F	CGCAAGCTTTGTTGAAAGTTAAACTTGATTTTG
Onsen LTR_BamHI-R	CGCGGATCCTGTTAGAGTAAAATTCTTTTAGAG
Onsen Gag_BamHI-F	CGCGGATCCATGAGAGACTCAAGAAAGAGAGAC
Onsen Gag_XhoI-R	CGCCTCGAGATCTTCTTTCTTCTTCTTCTTTTC
AtALKBH9B CDS_SpeI-F	CGGACTAGTATGGAAAACGATCCATTTCTCCG
AtALKBH9B CDS_XhoI-R	CCGCTCGAGACCGTAGTTTCTTCTACTAGGACG
*atalkbh9b*_sgRNA1-top	ATTGTCTCCGGCAGTACCAGCCGT
*atalkbh9b*_sgRNA1-bottom	AAACACGGCTGGTACTGCCGGAGA
*atalkbh9b*_sgRNA2-top	ATTGCTTCGGAGTTTCTGACGAAT

*atalkbh9b*_sgRNA2-bottom	AAAGATTCGTCAGAAACTCCGAAG
*atalkbh9b*_sgRNA3-top	ATTGTTTATCTAAAGATCTATGCA
*atalkbh9b*_sgRNA3-bottom	AAAGTGCATAGATCTTTAGATAAA
pET28a_*Onsen* Gag-F	ACAGCAAATGGGTCGCATGAGAGACTCAAGAAAG
pET28a_*Onsen* Gag-R	CGACGGAGCTCGAATTCGGATCCATCTTCTTTCTTCTTC
JW771_9B-F	TTTGGAGAGAACACGGGGGACATGGAAAACGATCCATT
JW771_9B-R	TAGTCCATTTGTTGGATCCCGACCGTAGTTTCTTCTACTA
JW772_ECT2-F	CGAGAAGCTCGAGTATCTTTTAAAACAAAAGAGGA
JW772_ECT2-R	GATACGAACGAAAGCTCGGCAAGATAGATCAAAA
JW772_UBP1b-F	CGAGAAGCTCGAGTATATGCAGAGGTTGAAGCAG
JW772_UBP1b-F	GATACGAACGAAAGCTTTACTGGTAGTACATGAG
JW772_PAB2-F	TCTCGTACGCGTCCCGGGGCCAACGGCTGAGATCAAT
JW772_PAB2-R	CCGATGATACGAACGAAAGCTTTAAAGTTTAAAATGTAT TTCTT
UBP1b gDNA_XmaI-F	TATAAGGTCGACCCCGGGATGCAGAGGTTGAAGCAGCA
UBP1b gDNA_SpeI-R	AATTCGAGCTCACTAGTTTACTGGTAGTACATGAGCTGC T

In vitro Transcription

Onsen fragment PCR-F	TAATACGACTCACTATAGGGCCACCATGCTCCTAGCAAC AAAAAATTTGAG
Onsen fragment PCR-R	ATCGAATGAGAATGTTTCCTTTACCT

ddPCR

Onsen ddPCR-F	GAAAAGAAGAAGAAGAAAGAAGATAT
Onsen ddPCR-R	CCATTTCCATATCCACCACG
CBF2 ddPCR-F	CTTCGGCCATGTTATCCAAC
CBF2 ddPCR-R	TTTATACGCCGGAACAGAGC
Onsen ddPCR-Probe	TAGACATCCCCAACATCGCCTCTTCAT (5'-HEX, 3'-BHQ1)
CBF2 ddPCR-Probe	CCAAAGTTACCAAAGAAGAGGTGGTGGT (5'-FAM, 3'-BHQ1)

ALE-qPCR

Adaptor_ALE-top	AGAGAGTAATACGACTCACTATAGGGACACGACGCTCTT CCGATCT
Adaptor_ALE-bottom	AGATCGGAAGAGCGTCGTGTCCCTATAGTGAGTCGTATT ACTCTCT (5'-phos)
ALE RT primer	AGACGTGTGCTCTTCCGATCTGCTCTGATACCA
Evade full length-F	TATTGATCAAGACTCAAATAAGAAAG
Evade full length-R	AAGAGTGAGATAGATCCACAAG
Onsen ALE_qPCR-F	CCGATCTTGTTGAAAGTTAAACT
Onsen ALE_qPCR-R	TCTAGAACTTGGATTTGGCC
Evade ALE_qPCR-F	TCCGATCTTATTGATCAAGAC
Evade ALE_qPCR-R	AGACTTCTCATATGTTCGGC

Quantitative PCR	
*Actin2*_qPCR-F	GGTAACATTGTGCTCAGTGGTGG
*Actin2*_qPCR-R	CAACGACCTTAATCTTCATGCTGC
*AtALKBH9B*_ qPCR-F	GGGATCAGTTCTGGTGTTAAATGG
*AtALKBH9B*_ qPCR-R	CGTTTCGACTCATCCATTTTCCTA
AT2G05632_qPCR-F	GTGAGATTGTTAGATCAGGAGAGT
AT2G05632_qPCR-R	ACAAGAAATCCCGACGGTAAA
AT5G09460_qPCR-F	AGCACTGTTGATGGTCCACTTCTT
AT5G09460_qPCR-R	TCTCAGAGCGGTGTGAATCTTGTC
AT4TE85370_qPCR-F	TCATTTCGAGGGATAGAGTGAA
AT4TE85370_qPCR-R	CTCCATTAACGGAGCTCCAT
*CCR2*_qPCR-F	CGTCCGGTGATGTTGAGTATCG
*CCR2*_qPCR-R	TCTTGGAATCAATAACGTCGCCG
m^{6}A_region A_qPCR-F	TTAAAATATTTTAGATATTTTGTAGTT
m^{6}A _region A_qPCR-R	TTAAGTGTTTTGAGAGAGTTTTTT
m^{6}A _region B_qPCR-F	CAAGTGTCAAATGCTACAATTGTG
m^{6}A _region B_qPCR-R	CTCAAATTTTTTGTTGCTAGGAG
m^{6}A _region C_qPCR-F	GAGAAGGCCAACTACGTTGAA
m^{6}A _region C_qPCR-R	ACCACTTATGATTCTCTTTTTGTTC

Table S3. Oligonucleotide sequences used in this study.

Sequences of oligonucleotides are provided. F, forward primer; R, reverse primer.

Sample	Clean Reads	Uniquely mapped	Multiple mapped	Alignment rate (%)
RNA-seq HS Col-0 rep 1	54631142	50931042	1554006	96.07
RNA-seq HS Col-0 rep 2	49530568	46331424	1450804	96.47
RNA-seq HS Col-0 rep3	56941182	53027774	1631766	95.99
RNA-seq HS *atalkbh9b-1* rep 1	45239018	41833150	1357700	95.47
RNA-seq HS *atalkbh9b-1* rep 2	47123274	43531676	1368852	95.28
RNA-seq HS *atalkbh9b-1* rep 3	47327074	43750278	1423692	95.45
SG-RNA-seq HS Col-0 rep 1	48668586	31889498	4468366	74.70
SG-RNA-seq HS Col-0 rep 2	43569356	29263934	3668906	75.59
SG-RNA-seq HS Col-0 rep 3	46027924	31150946	3602644	75.51
SG-RNA-seq HS *atalkbh9b-1* rep 1	35964564	10495688	1938240	34.57
SG-RNA-seq HS *atalkbh9b-1* rep 2	35522672	8915518	1436312	29.14
SG-RNA-seq HS *atalkbh9b-1* rep 3	34070430	9928480	1791304	34.40
ONT-DRS HS Col-0	316066	232324	62233	93.19
ONT-DRS Col-0 total (reference to Col-0 SG)	858535	592373	63126	76.35
ONT-DRS *atalkbh9b-1* total (reference to *atalkbh9b-1* SG)	519947	395516	51574	85.99
ONT-DRS Col-0 SG fraction	1450532	525654	219800	51.39
ONT DRS *atalkbh9b-1* SG fraction	1167183	461341	179635	54.92

Table S4. Summary of NGS data.

Read numbers and alignment rates of sequencing data are provided. HS, heat stress; SG, stress granule; ONT-DRS, Oxford Nanopore Technologies direct RNA sequencing; rep, replication.

Supplementary Excel File. Raw data and images used in the figures.

The Excel file associated to this paper includes all the raw data and uncropped images that are used to generate the figures presented in this study.